Anthropogenic and biogenic pollutants in a forested environment: SPRUCE-22 campaign overview

Angeliki Matrali, Christina Vasilakopoulou, Andreas Aktypis, Christos Kaltsonoudis, Kalliopi Florou, Agata Blaziak, David Patoulias, Evangelia Kostenidou, Kacper Blaziak, Katerina Seitanidi, et al.

Anthropogenic and biogenic pollutants in a forested environment: SPRUCE-22 campaign overview

Angeliki Matrali[1,2], Christina N. Vasilakopoulou[1,2], Andreas Aktypis[1,2], Christos Kaltsonoudis[2], Kalliopi Florou[2], Agata Błaziak[3], David Patoulias[2], Evangelia Kostenidou[4], Kacper Błaziak[5,6], Katerina Seitanidi[2], Ksakousti Skyllakou[2], Yoann Fagault[7], Thibaut Tuna[7], Christos Panagiotopoulos[8,9], Edouard Bard[7], Athanasios Nenes[2,9], Spyros N. Pandis[1,2]

[1]Department of Chemical Engineering, University of Patras, Patras, Greece
[2]Institute of Chemical Engineering Sciences, ICE-HT, Patras, Greece
[3]Institute of Physical Chemistry, Polish Academy of Sciences, Warsaw, Poland
[4]Department of Environmental Engineering, Democritus University of Thrace, Xanthi, Greece
[5]University of Warsaw, Faculty of Chemistry, Warsaw, Poland
[6]Biological and Chemical Research Center, University of Warsaw, ul. Żwirki i Wigury 101, 01-224 Warsaw, Poland
[7]CEREGE, Aix Marseille Universitè, CNRS, IRD, INRAE, Collège de France, Technopole de l'Arbois BP 80, 13545 Aix-en-Provence, France
[8]Aix Marseille Univ, Université de Toulon, CNRS, IRD, MIO, Marseille, France
[9]School of Architecture, Civil and Environmental Engineering, Ecole Polytechnique Fédérale de Lausanne, Lausanne 1015, Switzerland.

Corresponding author. Department of Chemical Engineering, University of Patras, Patras, GR, 26500, Greece. E-mail address: spyros@chemeng.upatras.gr (S. N. Pandis).

Abstract

The SPRUCE-22 field campaign was conducted during July 2022 on a remote mountainous forested site in Greece to assess interactions of biogenic and anthropogenic pollutants in the Eastern Mediterranean. Particle chemical composition and size distributions along with concentrations of organic and inorganic gases were measured at high temporal resolution, while samples were collected and analyzed off-line. PM_1 had a surprisingly high average concentration of 13 μg m^{-3} consisting primarily of organics (57%), followed by sulfate (30%), ammonium (9%), and black carbon (2%). Nitrates (both inorganic and organic) were less than 1% of the PM_1 despite the relatively high NO_x emissions in the Balkans. The $PM_{2.5}$ concentrations at this remote site were similar and even higher than those in major cities across Greece including Athens, indicating the importance of regional transport for summertime pollution in the Eastern Mediterranean. The relatively constant average diurnal profiles of major anthropogenic pollutants are consistent with only minimal effects from local sources.

Sulfates are not any more the dominant component of fine PM in Greece due to the reduction of SO_2 emissions of coal-burning powerplants. The organic aerosol (OA) was quite oxidized with an average oxygen to carbon ratio (O:C) equal to 0.83. The average concentration of isoprene was 0.6 ppb, of monoterpenes 0.5 ppb, while the biogenic secondary organic aerosol factor (obtained through source apportionment analysis) was estimated to contribute 22% of the OA. Additional biogenic secondary organic aerosol (SOA) may be part of the two oxygenated OA (OOA) factors that were also identified. Radiocarbon analysis indicated that the non-fossil carbon was approximately equal to the sum of the biogenic and the more oxidized oxygenated OA, implying that the less oxidized OOA in this study was mostly associated to anthropogenic fossil fuel combustion. The biogenic SOA was quite aged (O:C equal to 0.63) and was also mostly transported to the site. Nearby new particle formation events occurred during 20 % of the days, with an average SO_2 concentration of 0.3 ppb. The oxidative potential of the PM per unit of mass was quite high. The source attribution of the fine PM and the interactions among its anthropogenic and biogenic components are also discussed.

1. Introduction

The airborne particulate matter (PM) effects on human health (Pope et al., 2006) and climate have motivated investigations of the atmospheric processes that govern its formation and evolution as well as its physical, chemical and toxicological properties. Field campaigns that characterize the levels and variations of atmospheric pollutants at one or more sites, allow the evaluation of atmospheric chemical transport models and help identify important processes that can be further studied in laboratory experiments. The Mediterranean region is an interesting study area due to the abundance of different sources (urban and biogenic continental emissions, semi enclosed marine environment with influences from desert dust). During summer, limited wet removal (due to low precipitation) and increased solar radiation promoting oxidant formation (O_3, OH) lead to increased levels of secondary PM in the area (Bougiatioti et al., 2014; Dayan et al., 2017; Cristofanelli et al., 2016).

A number of studies have focused on fine (PM_1) and coarse (PM_{10}) particle composition and their sources on continental or regional background sites across the Mediterranean. Mallet et al. (2019) gathered chemical composition observations for fine particulate matter (PM_1) across the Mediterranean during spring and summer, where it can be noted that in the eastern region sulfate was the dominant PM_1 component due to increased SO_2 emissions. In contrast, the western part PM_1 was dominated by organics. A significant portion of the observed organic

aerosol is highly oxidized and is termed oxidized organic aerosol (OOA) creating a background of PM for a broad area (Jimenez et al., 2009).

The remote background station of Finokalia has provided information about the regional background of Eastern Mediterranean for 30 years (Gialesakis et al., 2023; Sciare et al. 2003). Sciare et al. (2003) reported daily concentrations of non-sea salt sulfate up to more than 8 μg m^{-3} during summertime. The bulk PM ammonium/non-sea salt sulfate equivalent ratio was on an average 1.49, indicating strongly acidic particles. A year later, during the MINOS campaign in August (Sciare et al., 2005) the fine PM measured was on average 17.4 μg m^{-3} comprised primarily of ammonium sulfate (45%) and organics (45%). In both summertime FAME campaigns (May to June 2008 and 2016) (Pikridas et al., 2010; Florou et al. 2024) the sulfate fraction of the PM_1 was dominant at 50% and 45% respectively, while the organics contributed 28% and 35% respectively. In both cases the organics were primarily secondary and highly aged. During the summer 2012, Bougiatioti et al. (2014) reported equal contributions of sulfate and organics in Finokalia to the 12 μg m^{-3} average PM_1 levels. The organic aerosol was again highly oxygenated and processed, with the study highlighting the influence of aged biomass burning plumes reaching the site.

Summertime wildfires are a common occurrence in the Mediterranean region, influencing air quality even far away, due to production of secondary OA, but also sulfates and nitrates (Diapouli et al., 2014). PM components associated with biomass burning and used for source attribution, like levoglucosan, are lost after atmospheric aging of a day under summertime conditions in the Eastern Mediterranean (Bougiatioti et al., 2014; Vasilakopoulou et al., 2023). In this way the organic chemical footprint of biomass burning PM is rapidly lost. Instead, aged biomass burning plumes appear as highly oxidized organic material and correlate better with inert species like fine K^+ and BC (Vasilakopoulou et al., 2023). Processed biomass burning emissions make up a large fraction of the observed summertime OA in the Mediterranean with Bougiatioti et al. (2014) reporting that 30% of organics in Finokalia were processed biomass burning OA (bbOA). Bossioli et al. (2016) estimated that fires in Turkey led to a 95% increase of the OA over the southeastern Aegean Sea under appropriate transport conditions.

Other studies have targeted the interactions of anthropogenic pollution with biogenic components when mixed. The Southern Oxidant and Aerosol Study (SOAS) campaign (Budisulistiorini et al., 2015) in a forested elevated site in Tennessee US, influenced by anthropogenic emissions, focused on isoprene interaction with anthropogenic pollutants. Approximately 10% of the observed OA was due to measured isoprene epoxydiol (IEPOX) related secondary organic aerosol (SOA), while positive matrix factorization (PMF) analysis

attributed 32% of the OA to an IEPOX OA factor. The source apportionment yielded no contribution from primary emissions, while one OOA factor was connected to biogenic emissions. The total OA of that study was quite oxidized with an O:C of 0.77. A relationship was found between anthropogenic sulfate and isoprene SOA, though no connection was observed between isoprene SOA and acidity (Budisulistiorini et al., 2015).

The SPRUCE campaign (Summer PeRtoUli Campaign Emissions) was conducted in 2022, aiming at the characterization of air quality in a remote forested area in the Eastern Mediterranean using an array of in-situ measurements and oxidation experiments as well as offline analysis of collected samples. The present paper acts as an overview, presenting the composition of the gas and particulate phase pollutants. Assessment of contributing sources to the observed PM_1 is presented and the influence of anthropogenic activity on this forested site is discussed. The magnitude of local organic production in this site, during summer was estimated, along with the frequency of new particle formation events in this environment. Finally, the air quality of this background site was related to the rest of the Greek mainland for the period examined, with respect to their PM levels.

2. Measurements

2.1 Site description

The campaign took place in a mountainous area in the mainland of Greece. The selected station was located at the chalet on top of the ski resort of Pertouli (39.545623, 21.498516) at an elevation of 1300 m above sea level. The closest anthropogenic source was the nearest village of Pertouli (80 inhabitants), located 3 km away and Trikala (81,400 inhabitants), the largest town in the region, is 50 km from the site, while the nearest road is 1 km away. The broad area includes a forest of fir trees (dominated by the Abies borisii-regis species), along with beech, oak and pine trees. The forest is especially dense within a 2 km radius from the site (Figure S1).

The majority of the instrumentation was placed inside the chalet. The sampling lines used were either made of Teflon (for gas phase analyzers) or copper (for the particulates). Sampling took place 8 m above ground. $PM_{2.5}$ heads were used to cut off larger particles. The FORTH mobile laboratory was used to house additional instruments. The inlet sampling lines protruded from the front of the van at about 3 m above ground.

2.2 Instrumentation

The month-long campaign took place from July 2 to August 2, 2022. Information on instruments deployed is provided in Table 1.

Table 1. Pollutants measured during SPRUCE-22 and corresponding average concentrations.

Pollutant	Average Concentration		Time Resolution	Instrument
PM_1	12.65±5.17	μg m^{-3}	3 min	HR-ToF-AMS (Aerodyne) *
PM_1	13.19±5.27	μg m^{-3}	3 min	SMPS*
N_4	3528±1615	cm^{-3}	3 min	SMPS
N_7	2815±1517	cm^{-3}	1 min	WCPC (TSI model 3789)
OA (PM_1)	7.44±3.19	μg m^{-3}	3 min	HR-ToF-AMS (Aerodyne) *
OC ($PM_{2.5}$)	3.74±0.95	μg m^{-3}	1 d	Sunset OC/EC
BC ($PM_{2.5}$)	0.26±0.12	μg m^{-3}	1 min	MAAP (Thermo Scientific Inc., 5012)
BC ($PM_{2.5}$)	0.42±0.18	μg m^{-3}	1 min	Aethalometer (AE33, Magee Scientific)
BC (PM_1)	0.15±0.07	μg m^{-3}	1 min	SP2-xr (Droplet measurement Technologies, DMT)
EC ($PM_{2.5}$)	0.11±0.07	μg m^{-3}	1 d	Sunset Lab OCEC Analyzer
Sulfate (PM_1)	3.84±1.74	μg m^{-3}	3 min	HR-ToF-AMS (Aerodyne) *
Ammonium (PM_1)	1.23±0.55	μg m^{-3}	3 min	HR-ToF-AMS (Aerodyne) *
Ammonium ($PM_{2.5}$)	1.73±0.56	μg m^{-3}	1 d	IC (Shimadzu, LC-20ADSP)
Nitrate (PM_1)	0.12±0.05	μg m^{-3}	3 min	HR-ToF-AMS (Aerodyne) *
Nitrate ($PM_{2.5}$)	0.51±0.14	μg m^{-3}	1 d	IC (Shimadzu, LC-20ADSP)
K^+ (PM_1)**	0.08±0.09	μg m^{-3}	3 min	HR-ToF-AMS (Aerodyne) *
K^+ ($PM_{2.5}$)	0.12±0.07	μg m^{-3}	1 d	XRF
Ca^{2+} ($PM_{2.5}$)	0.23±0.17	μg m^{-3}	1 d	XRF
Cl^-(PM_1)	0.025±0.005	μg m^{-3}	3 min	HR-ToF-AMS (Aerodyne) *
Cl^- ($PM_{2.5}$)	0.07±0.04	μg m^{-3}	1 d	XRF
Cu^{2+} ($PM_{2.5}$)	0.13±0.09	μg m^{-3}	1 d	XRF
O_3	64.9±8.3	ppb	1 min	TELEDYNE API (T400) *
SO_2	0.27±0.30	ppb	1 min	Pulsed Fluorescence Analyzer (Thermo, 43 i)
NO_2	1.75±0.62	ppb	1 min	Serinus 40 (ECOTECH)
Acetonitrile	0.10±0.05	ppb	10 s	PTR-QMS (IONICON)*
Methylvinylketone (MVK)	0.49±0.40	ppb	10 s	PTR-QMS (IONICON)*
Acetone	2.07±0.66	ppb	10 s	PTR-QMS (IONICON)*
Toluene	0.002±0.055	ppb	10 s	PTR-QMS (IONICON)*
Monoterpenes	0.490±0.77	ppb	10 s	PTR-QMS (IONICON)*
Isoprene	0.62±1.09	ppb	10 s	PTR-QMS (IONICON)*
Methyl ethyl ketone (MEK)	0.16±0.10	ppb	10 s	PTR-QMS (IONICON)*
Benzene	0.04±0.03	ppb	10 s	PTR-QMS (IONICON)*
Acetone	2.13±0.75	ppb	10 s	PTR-QMS (IONICON)*
Acetic acid	0.51±0.39	ppb	10 s	PTR-QMS (IONICON)*

*Instruments in the FORTH mobile laboratory, also used in dual chamber experiments. During the periods of the smog chamber experiments those did not collect ambient measurements, resulting in a partial deficit in the ambient dataset.
**The AMS measures only a fraction of the K^+

A High-Resolution Aerosol Mass Spectrometer (HR-Tof-AMS, Aerodyne) was operated with no dryer, providing PM_1 chemical composition measurements. The instrument background was monitored daily with the use of a HEPA filter at the inlet for approximately 30 min. The AMS was calibrated with ammonium nitrate at the beginning of the campaign.

Three scanning mobility particle sizers (SMPS) were used, and their measurements were combined to cover the size range from 4 to 710 nm. SMPS#1 complimented the measurements of the AMS inside the FORTH mobile lab and was comprised by a TSI classifier (model 3080), a differential mobility analyzer (DMA) measuring sizes of 14-710 nm (TSI 3081 model) and a TSI 3775 butanol condensation particle counter (CPC). It operated on an aerosol flow rate of 0.6 L min^{-1} with a sheath flow of 3 L min^{-1}. SMPS#2, operating inside the chalet, differed from SMPS#1 only in the use of a water CPC (TSI model 3787) instead of a butanol one. Finally, SMPS#3 (classifier: 3080 TSI, CPC: TSI 3775) used the DMA model 3085 of TSI spanning ranges of 4-118 nm and sampled with a flowrate of 1.5 L min^{-1} (sheath flow of 5 L min^{-1}) from inside the chalet.

Black carbon was monitored by a Multi-Angle Absorption Photometer (MAAP model 5012, Thermo Scientific) and an Aethalometer (Model AE33, Magee Scientific), using a $PM_{2.5}$ cutoff head. Also, a Single Particle Soot Photometer (SP_2-xr, DMT) was operated on site. $PM_{2.5}$ mass concentrations were measured through a low-cost Purple Air monitor.

Concentrations of volatile organic compounds (VOCs) were measured by proton transfer reaction mass spectrometry by a quadrupole PTR-MS (PTR-QMS 500, Ionicon Analytik). Correcting for background instrument signal required sampling through an activated charcoal filter (Supelco Analytics) each day for 30 min. The instrument was calibrated on site at the beginning of the campaign with the use of a precision calibrator (model 702, Teledyne Inc.) for dilution of a standard gas VOC mixture (15 compounds, Restek). Response factors can be found in Table S1. The calibration mix had VOC concentrations of 1 ppm and was used with a dilution factor of 40 (~25 ppb).

Measurements of inorganic trace gases included NO_2 (Ecotech, Serinus 40), SO_2 (Thermo 43 i) and O_3 (Teledyne, T400). The analyzers were zeroed using synthetic air at the beginning of the campaign.

Along with the online instrumentation, particulate and gas phase samples were collected daily for the duration of the campaign. Stainless steel sorbent tubes (3.5” x 0.25” packed with

Tenax^{TA}, Markes International®) were installed in a custom-made sampler operating at a flow of 0.1 L min^{-1}. No scrubber was used prior to the sorbent tubes for the removal of oxidants. The retained organic compounds were analyzed with the use of gas chromatography mass spectrometry (GCMS, Shimadzu model QP2010) after a two-step desorption via a cold trap in a thermal desorber (Markes International Ltd, UNITY–Air Server-xr).

For particulates, $PM_{2.5}$ samples were collected on 101.6 mm Quartz filters (Pall LifeSciences) on a medium flow sampler operating at 110 and 160 L min^{-1} (Tisch Environmental, TE-1000). The filters were subsequently cut into punches for use in different analytical techniques.

Both the sorbent tubes and the filters were conditioned before deployment to minimize artifacts (sorbent tubes at 300 ^{o}C for 10 min and filters for 4 h at 500 ^{o}C). To further minimize potential artifacts, field blanks were used, and the samples were kept in a freezer to additionally minimize loss of analytes.

A thermal optical method (protocol NIOSH 870, Panteliadis et al., 2015) was used by a Sunset OC/EC analyzer (Sunset Laboratory Inc.) for the filter-based measurements of organic carbon (OC). A solution of sucrose was applied into a filter punch and analyzed to verify the calibration of the system.

The oxidative potential (OP) of the water-soluble fraction of the fine aerosol was measured in an effort to assess its potential toxicity. The dithiothreitol (DTT) assay was used following the approach described in Georgopoulou et al. (2024).

Radiocarbon measurements were conducted in Aix-en-Provence using an elemental analyzer (EA) coupled to the gas interface system (GIS) of the AixMICADAS system (Bard et al., 2015). In short, two filter punches (1.5 cm^2 each) were transferred into silver capsules (8 x 8 x 16 mm, Elementar Analysensysteme GmbH) previously prebaked at 800°C for 2 hours to minimize contamination by extraneous carbon adsorbed at the surface of the vessels (Bonvalot et al., 2016). The filters were then impregnated with 200 µL HCl (1 N) to eliminate potential carbonates present in the aerosols. After the acidification step was carried out in a laminar flow hood, the samples were immediately placed in a polypropylene glove box continuously fed with nitrogen for a minimum of 1 hour before being dried at 80°C under a nitrogen stream (Reacti-Vap™, Thermo Fisher Scientific Inc). Following decarbonatation, the samples were stored in 2 ml glass vials treated at 500°C for 2 hours and closed with screw caps with septa silicon/PTFE. The samples were analysed within 2 weeks using the EA-GIS-AMS parameters described elsewhere (Bonvalot et al., 2016; Tuna et al., 2018). The measurements were normalized with OxA2 standard gas (≈100 µgC; CO_2 produced from NIST Oxalic Acid II,

NIST SRM4990C). A ^{14}C free CO_2 gas canister (≈100 μgC) was used to correct the blanks for OxA2 standard gas whereas samples were corrected for procedural blanks.

2.3. Data Analysis

The origin of the air masses arriving at the site was determined by the Single-Particle Lagrangian Integrated Trajectory model HYSPLIT (Draxler and Hess, 1998) and the particle dispersion model FLEXPART (Stohl et al., 2005) both in backward mode. HYSPLIT backward trajectory analysis was conducted using meteorological input from the GFS model (0.25° spatial resolution) with an endpoint 50 m above ground level. Categorization of the regional sources was based on clustering analysis using the Openair R package (Carslaw and Ropkins, 2012), using as input the 48 h backward trajectories. The chosen method for grouping the data employed 3 clusters and the angle distance matrix, clustering trajectories based on the angle of their origin with respect to the site. Clusters were also tested with both the angle and Euclidean distance methods (grouping based on distance of the trajectories' origin coordinates) and the results were effectively similar.

The AMS dataset was analyzed using the SeQUential Igor data RetRiEvaL (SQUIRREL) v1.57I and Peak Integration by Key Analysis (PIKA) v1.16I both written in Igor Pro (WaveMetrics, Lake Oswego, OR). The Canagaratna et al. (2015) method was used to determine the elemental ratios (e.g O:C, H:C) of the organic fraction of the aerosol. The AMS measurements were corrected for the collection efficiency (CE) of the instrument with the use of the Kostenidou et al. (2007) algorithm with an interval of 2-3 hours with the use of the collocated SMPS size distribution measurements. The average CE was 0.80 ± 0.16. The density of the OA was also estimated by the same algorithm. The fraction of the nitrate group that was related to organic nitrates was determined as described by Kiendler-Scharr et al. (2016). Positive matrix factorization (PMF, Paatero and Tapper, 1994) was applied to the high-resolution mass spectra (*m/z* range of 12-200) of the organic aerosol (OA). The values of the $PM_{2.5}$ from the low-cost sensor were corrected following Kosmopoulos et al. (2022).

The concentrations of VOCs were measured by the PTRMS. For the 14 compounds contained in the calibration mix their normalized (as to the hydronium ion) sensitivities were calculated by:

$$S_m = \frac{C_{RH,cal} - C_{RH,zero}}{C_{H_3O+,cal}\,500 + 0.5\,C_{H_3O+(H_2O),cal}}\,10^6\ [\text{ncps ppb}^{-1}] \quad (1)$$

where, C_{RH}, C_{H_3O+}, $C_{H_3O+(H_2O)}$ the counts per second for the analyte and the primary ions for either the zeroing or the calibration period. For the compounds included in the calibration mix, the ambient concentrations were calculated with the use of this sensitivity factor. For the rest of the monitored *m/z* values the operating conditions of the PTR drift tube were used for estimation of ambient concentrations using a rate constant of k=2.0×10^{-9} cm^3 s^{-1} for all the analytes (IONICON, 2020). Attribution of the signal *m/z* to compounds was made with use of fragmentation tables taking into account the analysis of the Tenax tubes.

For the radiocarbon analysis, due to the small carbon amount contained in the processing filters (around 0.3 µgC/cm^2 were determined separately by EA measurement), approximately 35 µgC of phthalic acid (^{14}C free blank) was added to the processing blanks. Because of elevated analytical costs and the limited number of blank filters, the blank correction was performed with a carbon mass representative of the aerosol samples (carbon masses ranging from 23 to 70 µgC with an average of 38 µgC and a standard deviation of 12 µgC). A relative error of 50% based on the measurements of 12 procedural blanks from 3 sampling campaigns was propagated to the procedural blank value obtained in this study (F^{14}C = 0.0284, N=2). An additional uncertainty of 2.2‰ was propagated in the error calculation to account for the long-term variability on OxA2 gas. Normalization and blank correction were performed using the BATS software (Wacker et al., 2010) and all measurements are expressed in F^{14}C as defined by Reimer et al. (2004).

As a first approximation, we assume that the carbonaceous fraction is composed of two endmembers: a fossil fraction free of ^{14}C, and a non-fossil fraction assumed to be isotopically homogenous. To determine this non-fossil fraction (f_{NF}), the measured F^{14}C has to be normalized by a non-fossil reference value ($f_{NF,ref}$, expressed in F ^{14}C) as described by:

$$f_{NF} = \frac{F^{14}C}{f_{NF,ref}} \quad (2)$$

In the present study, it is assumed that the non-fossil fraction can originate from biogenic and/or wood burning emissions with slightly different ^{14}C signatures. Biogenic emission should be close to the atmospheric ^{14}C level at the time of collection whereas wood burning emission have higher ^{14}C content due to the uptake during tree growth of CO_2 contaminated by ^{14}C from atmospheric thermonuclear tests that started in the late 1950s. Other source proxies may help to discriminate between both processes. As a first approximation, we have estimated two end-members for the non-fossil reference value: a lower bound ($f_{NF,ref}$ = 1.00) for biogenic carbon including modern (2022) atmospheric CO_2 and upper bound ($f_{NF,ref}$ = 1.04) for wood burning emission. This latter value was calculated by combining atmospheric data over the last decades

(Hua et al., 2022; Levin et al., 2022) and a tree-growth model (Lewis et al., 2004; Mohn et al., 2008) assuming an average tree age of 30 years for forest wildfires.

3. Results

3.1. Meteorology

The site was predominantly (51% of the time) affected by airmasses coming from the NE Balkans (Figure 1), which reached the site from the east passing over the northern Aegean Sea (Figure S2). Around 39% of the trajectories originated from the north passing over Serbia. The remaining 10% of the air masses came from the west, had lower wind speeds, and passed over the Ionian and the Adriatic Sea. Approximately, 6% of all the air masses are characterized as stagnant, since for 2 d prior to reaching the site, they remained within 200 km from it.

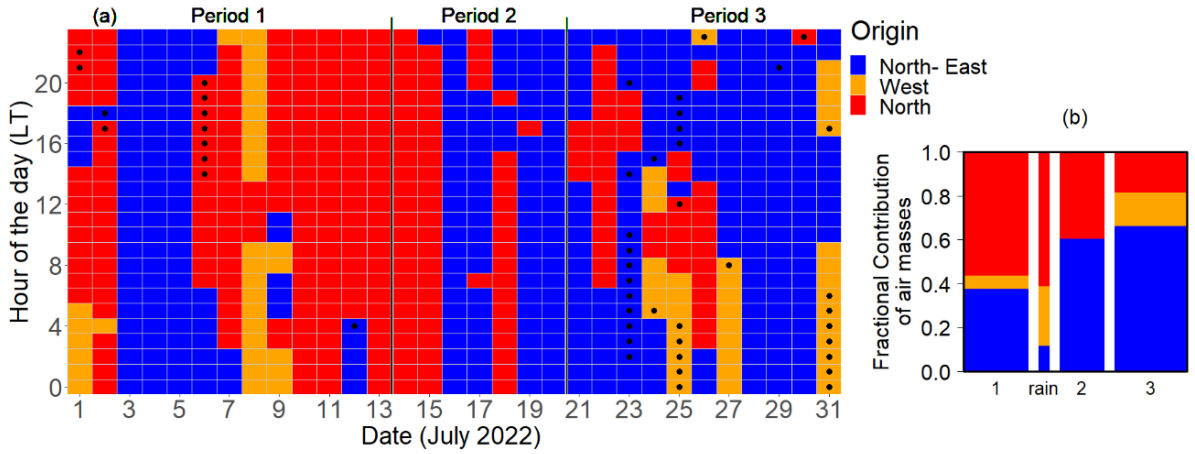

Figure 1. (a) Origin of air masses reaching the station at an elevation height of 50 m above the ground based on HYSPLIT. Colors indicate the origin of the 48 h backward trajectories, corresponding to three clusters coming from the North, the North-East and West. The black dots indicate stagnant air masses, which for 2 days remained within 200 km from the site. The black vertical lines define three subperiods in the campaign. (b) Fractional contribution of the clusters in each sub period, with size proportional to their duration. The rain period involves the period from July 8 midday to July 10 morning, when precipitation influenced pollutants' levels at the site.

The temperature during the campaign was mild at 20±5 ºC (hourly average), with a relative humidity of 57±16 % (Figure S3). The average increase in temperature during the day was in the order of 8 ºC (maximum at 15:00 LT), with a corresponding decrease in the RH of 20 %. There was one precipitation event accompanied by fog that lasted from midday of July 8 to morning of July 10 and resulted in significant removal of pollutants.

3.2. Concentration, composition, and properties of particles

The hourly PM_1 concentrations (summing the AMS and the MAAP measurements) for the entire campaign ranged from 0.7 (during the fog event) to 27 μg m^{-3} with an average value of 12.7±5.1 μg m^{-3} (Figure 2). The PM_1 was mostly comprised of organics (58.8%, with an average of 7.4±3.2 μg m^{-3}), whose density was 1.52 ± 0.29 g cm^{-3} as calculated from the Kostenidou et al. (2007) algorithm, using the combined AMS-SMPS dataset. Sulfate represented 30.3% of the PM_1 (average 3.8±1.7 μg m^{-3}). Ammonium constituted 9.7 % (1.2 ±1.4 μg m^{-3}), while PM_1 nitrate was <1% (0.12±0.05 μg m^{-3}), with about 85% being organonitrates (Figure S4). The $PM_{2.5}$ black carbon was 0.26±0.12 μg m^{-3} (2.1 %). It is assumed that most of the $PM_{2.5}$ BC was in the PM_1 range. PM_1 ammonium displayed excellent correlation to sulfate (R^2 = 0.98 for hourly averages, Figure S5).

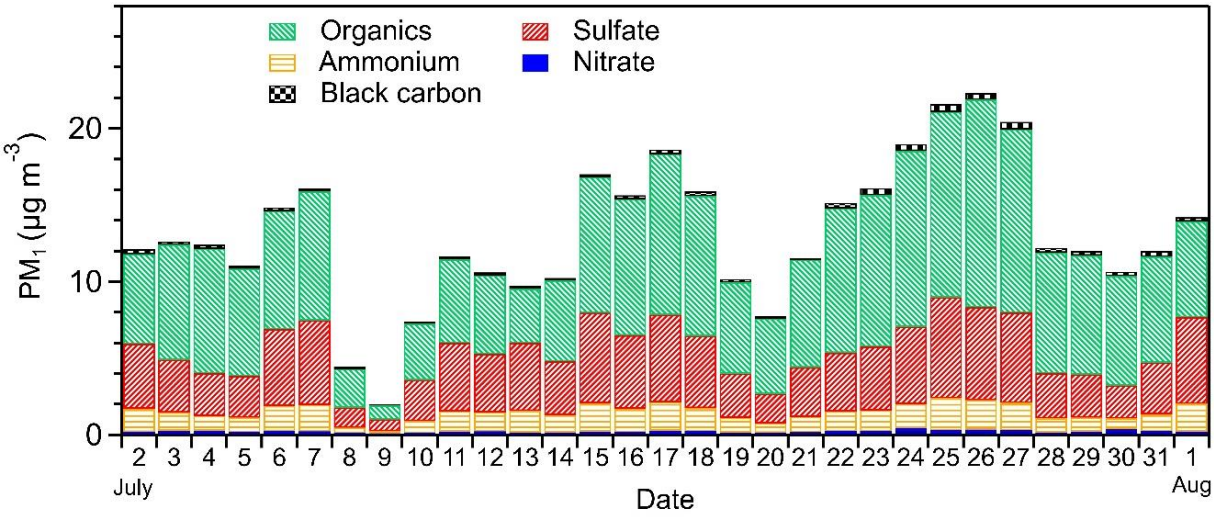

Figure 2. Daily average PM_1 chemical composition during the SPRUCE campaign, based on the AMS and the MAAP measurements.

The average mass distribution of all constituents peaked at a vacuum aerodynamic diameter of approximately 480 nm (Figure 3). However, across the campaign there was some differentiation in terms of the common peak of the mass distribution. During the period after the rain event (July 12 to 15) the distributions shifted to smaller sizes (peak at 374 nm), from the 460 nm that was the apex of the mass distribution at the beginning and during the precipitation event (Figure S6). From then on, the mode diameter was steadily increasing reaching 550 nm for after July 25. This variation could be the result of the wet removal of particulates in a broad area of the Balkans (Figure S7) that resulted in smaller particles that then progressively grew due to the formation of secondary PM.

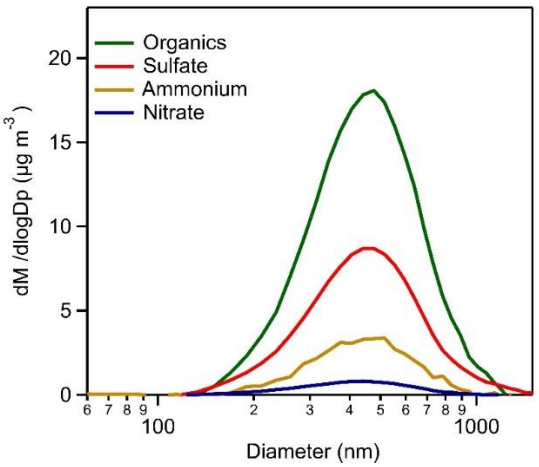

Figure 3. Average mass size distributions of major PM_1 constituents.

The OA was lowest when trajectories were coming from the North (median concentration of 6.6 μg m^{-3}) and higher for the Western air masses (median equal to 9.3 μg m^{-3}) (Figure S8). The differences were statistically significant. However, this variation in organics could be due to the progressive concentration increase during the campaign (with the first period dominated by the North air masses). On the other hand, sulfate was lower for the NE trajectories (median value of 3.50 μg m^{-3} as opposed to 4.35 μg m^{-3} for the western and 4.61 μg m^{-3} for the northern) but the difference in mean values was only statistically significant for the N-NE. This is probably due to the SO_2 emissions from major coal-fired power plants in northern Greece, Northern Macedonia, Bosnia/Herzegovina and Serbia (Figure S9). The Bulgarian power plants in the NE do not seem to contribute as much to the sulfate concentration observed at this site. Ammonium had similar behavior across all air masses as sulfate. Nitrate concentrations were low regardless of the air mass origin. Black carbon was slightly higher for the Western air masses (median of 0.38 μg m^{-3}) than the other two (0.24 for the N and 0.29 μg m^{-3} for the NE) following the trend of the organics.

Organics and sulfate were moderately correlated with R^2 =0.51 (0.39 with exclusion of the rain period) at an hourly resolution. The average OA/sulfate ratio was 2.1 ± 0.8 (Figure S10) and it exceeded 3 for several periods during the campaign, when the air masses had originated mainly from the NE and the W (Figure S11). The average OA/sulfate ratio from the NE and the W cluster was 2.8 and 2.6 respectively. The air masses from the north had the lowest mean OA/sulfate ratio of 1.6 as a result of the lower OA concentration and the slightly higher sulfates. There were very few hours (~30) during which the sulfate levels exceeded those of the OA (mainly on July 13).

The diurnally averaged PM_1 (Figure 4) increased from a minimum of 11.5 μg m^{-3} at 05:00 LT to 14.1 μg m^{-3} at 19:00 LT. The same fractional increase was observed for OA, which peaked at 18:00 LT. Sulfate displayed a small peak at 10:00 LT (equal to 4.2 μg m^{-3}) and a gradual increase peaking at 19:00 LT (from 3.6 μg m^{-3} at 12:00 LT to 4.3 μg m^{-3}). Ammonium had the same behavior as sulfate increasing from 1.2 μg m^{-3} at 12:00 LT to 1.4 μg m^{-3}. The concentration of nitrate slightly decreased during the day.

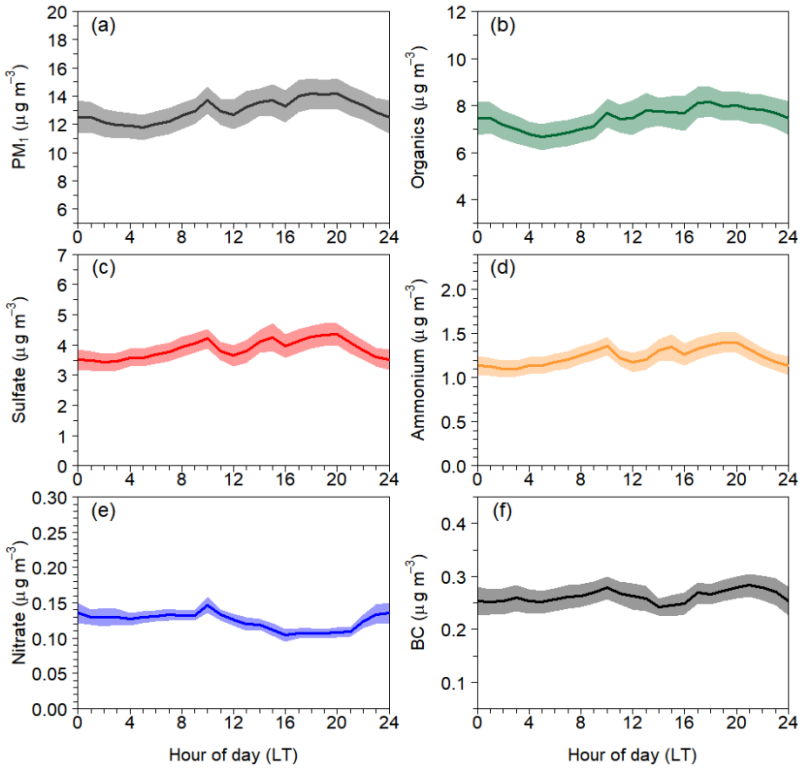

Figure 4. Diurnal variation of PM_1 concentrations and of major individual constituents. The shaded areas correspond to one standard deviation of the mean of the corresponding hourly values.

The black carbon (BC) concentration was relatively low throughout the campaign with hourly average values of 0.26 μg m^{-3} (Figure 5), as measured by the MAAP. Its concentration increased in the second part of the campaign along with the OA. The diurnal profile of BC was relatively flat with no more than 0.04 μg m^{-3} variation (13%) during the day (Figure 4f). This profile suggests negligible contributions from local sources. The measurements of the other two BC instruments (aethalometer and SP_2-XR) had high correlations (R^2 from 0.88 to 0.95) with the MAAP values. The aethalometer measured higher BC by 0.16±0.08 μg m^{-3} compared to the MAAP (aethalometer average BC of 0.42±0.18 μg m^{-3}), which is consistent with other studies (Tasoglou et al., 2018; Pikridas et al., 2019). The differences can probably be explained by the default mass absorption cross-section values used to derive the equivalent BC.

Significant coating effects on the BC absorption are expected in this environment in which the aerosol is quite aged (Zhang et al., 2023). In turn, the SP_2, measured lower concentrations than the MAAP by 0.10±0.08 μg m^{-3} (SP_2 average BC equal to 0.15±0.07 μg m^{-3}). Lower values of the refractive BC by about 50 % for aged PM have been also reported in past studies (Zhang et al., 2023).

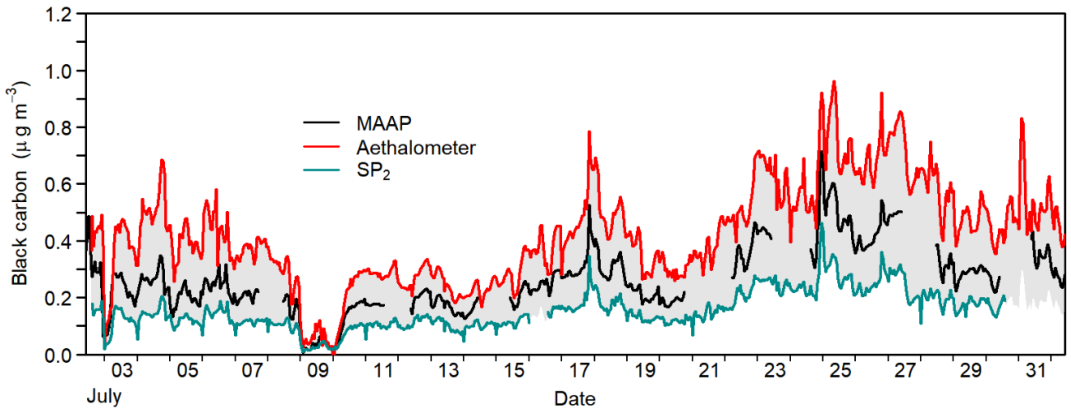

Figure 5. Hourly averaged concentrations of black carbon as measured by the various instruments during the campaign.

The average diurnal variation of the OA to BC ratio is shown in Figure 6a. The fact that the OA/BC increased by 22 % from 08:00 LT to 15:00 LT strongly suggests the presence of regional photochemistry and SOA production. There is also another peak at 23:00 LT during the nighttime.

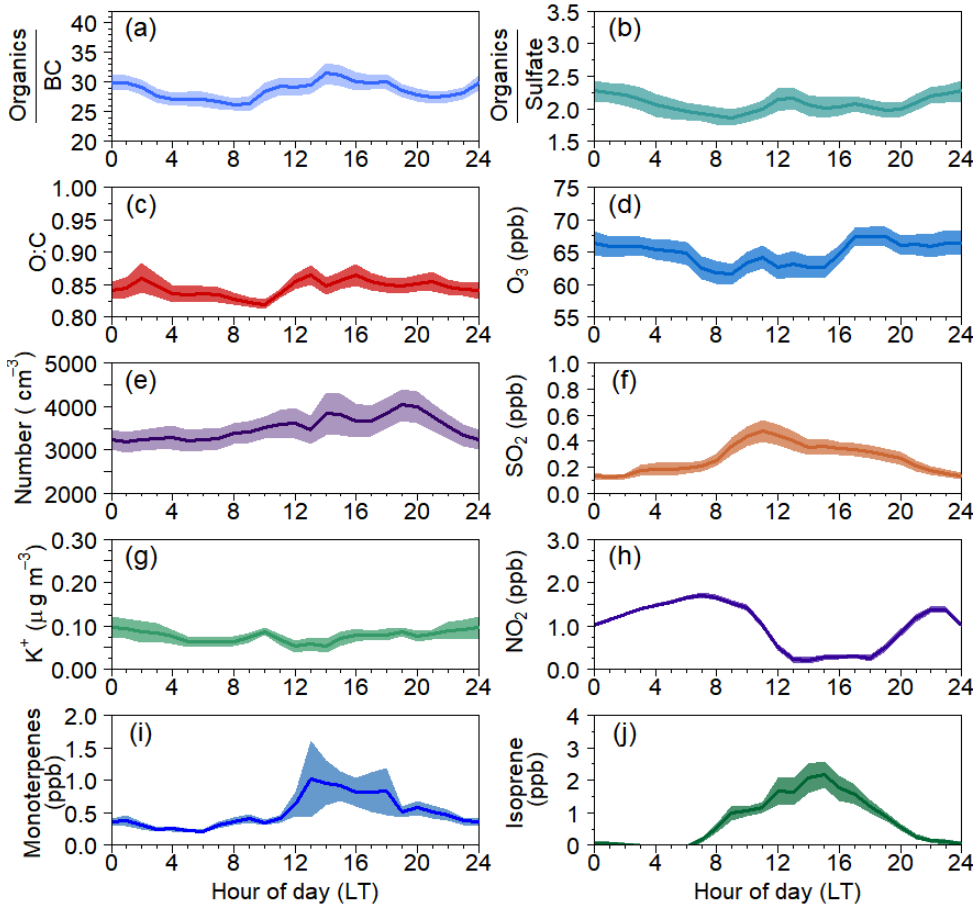

Figure 6. Diurnal variation of (a) organics to black carbon ratio (b) organics to sulfate ratio, (c) O:C ratio, (d) ozone, (e) N_4, (f) SO_2, (g) K^+, (h) NO_2, (i) monoterpenes, (j) isoprene. The shaded areas correspond to one standard deviation of the mean of the corresponding values.

The average O:C was 0.84 indicating highly oxygenated OA. The O:C was relatively stable throughout the campaign (Figure 7) with a notable decrease to a value of 0.62 at midnight of July 3, resulting from a general drop in PM concentrations (the OA decreased to 1.8 μg m^{-3} from 7 μg m^{-3}) due to a shift in air mass origin from the north to passing over the Aegean within 2 days before reaching the site (Figure S12). These air masses were probably cleaned by rain that removed very aged organics and were enriched afterwards with fresher OA with lower O:C. The average diurnal behavior shows a small variation in the O:C which increased by 0.05 (6%) from 0.82 to 0.87 from 10:00 LT to 13:00 LT probably due to regional photochemistry (Figure 6.c). The OA:OC ratio was ~2.3, similar to that observed at other Greek summer campaigns and indicative of aged aerosol (2.2 for Hildebrandt et al. (2010) in Finokalia).

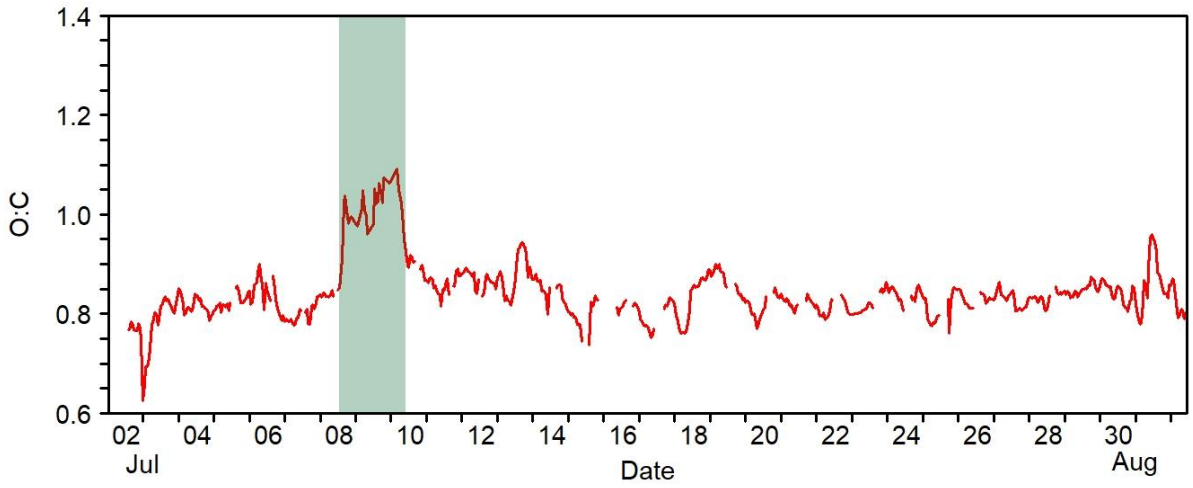

Figure 7. Hourly O:C ratio values of the PM_1 OA. The shaded area depicts the fog period.

The observed PM_1 composition is consistent with previous observations in the western Mediterranean for a similar period (Michoud et al., 2017; Minguillón et al., 2015). The decrease in the sulfate fraction that dominated PM_1 in past campaigns in the Eastern Mediterranean (for example Pikridas et al. (2010) reported that 50% of the PM_1 in Finokalia in 2008 was sulfate), stems from stricter regulations limiting SO_2 emissions and reducing the secondary sulfate (Urdiales-Flores et al., 2023). The low levels of nitrate (organic and inorganic) are mainly attributed to inorganic nitrate's volatilization under warm conditions (Voutsa et al., 2014; Ripoll et al., 2015) and to the dissociation of organic nitrates during aging (Kiendler-Scharr et al., 2016).

The $PM_{2.5}$ potassium (based on the XRF analysis of the filter samples) was on average equal to 0.12±0.07 μg m^{-3} and it was correlated with BC (R^2=0.65) and the more aged part of the OA (R^2=0.67 with the more oxidized factor, further discussed in the next section), due to its connection to wildfire emissions (Vasilakopoulou et al., 2023). Calcium had an average concentration of 0.24±014 μg m^{-3}, while copper and iron had 0.13±0.09 μg m^{-3} and 0.21±0.17 μg m^{-3} respectively.

The oxidative potential (OP), a known metric of aerosol toxicity, of the water-soluble components of the $PM_{2.5}$ was analyzed by Vasilakopoulou et al. (2023). Briefly, the average OP per unit of mass (DDT_m at 84 ± 27 pmol min^{-1}) was higher than literature-reported OP of oxidized OA in other Mediterranean sites. Expressed per volume of air the OP was 0.2 ± 0.03 nmol min^{-1} m^{-3} a value consistent with other European sites.

3.3. Sources of PM_1 OA

The positive matrix factorization (PMF) of the OA spectra by Vasilakopoulou et al. (2023), yielded 3 highly aged factors (Figure S13). The O:C ratio for the factors ranged from 0.63 for the biogenic oxygenated OA factor (bOOA), to 0.92 for the more oxidized one (MO-OOA), while the less oxidized organic factor (LO-OOA) had an O:C=0.84. This high O:C for the biogenic factor along with an only 20% increase in its diurnal profile during daytime (Figure S28) suggest that a large portion of this factor is transported to the site. The contribution of the factors changed across the campaign (Figure 8), with initial dominance of the LO-OOA (58% contribution to OA, up to July 14). From July 21 to Aug 1 the MO-OOA (54%) and bOOA (27%) dominated, while the period in between had contributions from all factors. Along the campaign's progression the factors seemed to also be connected to different individual organic compounds (Figure S14). The overall contribution of the LO-OOA and MO-OOA factors were similar at around 40%, with the biogenic contributing 22% to the OA for the whole campaign.

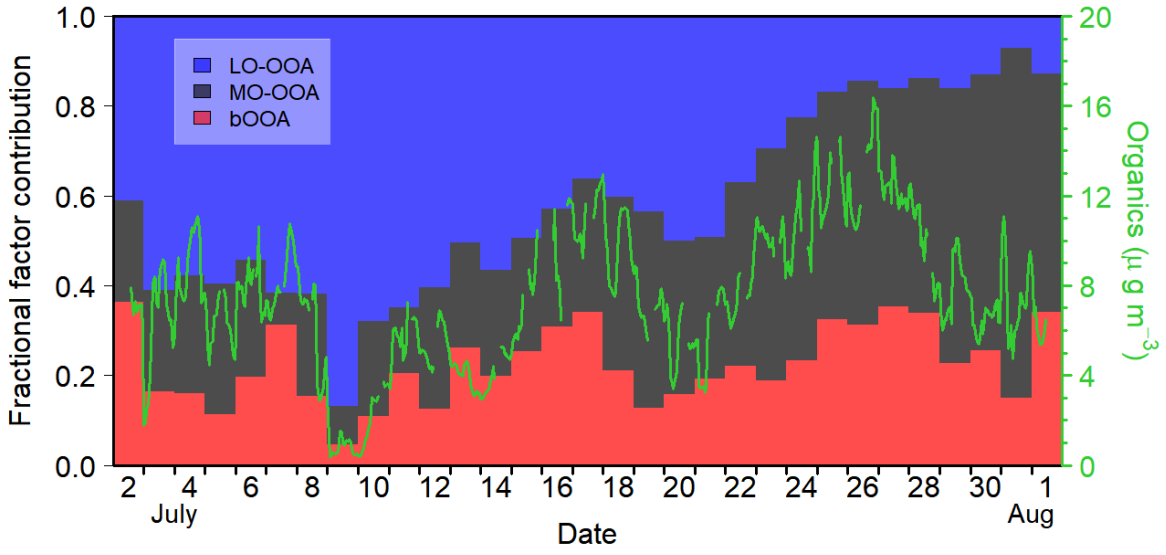

Figure 8. Daily fractional contribution of the factors to the observed OA for the SPRUCE campaign. The green line (right axis) depicts the hourly variations of the mass of the organics.

No significant link between the factors' concentration and the air mass origin was observed (Figure S15). The increased MO-OOA averages for the western sector are due to two fire plumes arriving within a couple of days to the site from Dadia, Greece (July 25) and Albania (July 31) (Vasilakopoulou et al., 2023, Figure S16). In general, the increased concentrations of MO-OOA for the period after July 22 were associated with aged fire plumes arriving from Portugal after a week of transport (Vasilakopoulou et al., 2023).

Radiocarbon analysis suggests that the non-fossil carbon fraction is quite close to the sum of the bOOA and the MO-OOA PMF factors (Figure 9). This observation strongly suggests that the more oxygenated factor observed on site does not include significant contributions from fossil fuel combustion, further supporting the hypothesis of Vasilakopoulou et al. (2023) that it consisted primarily of aged wildfire emissions.

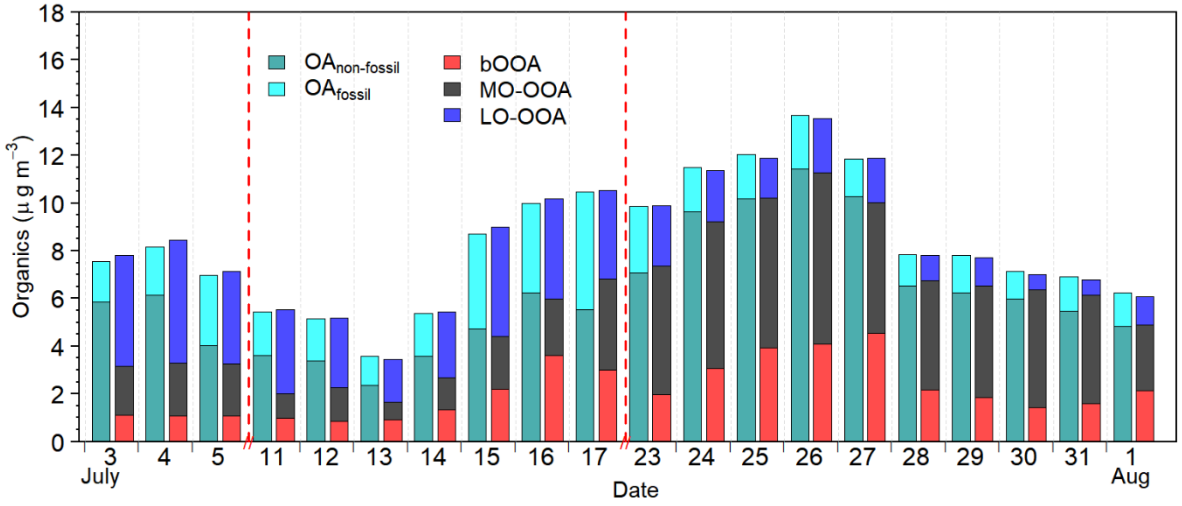

Figure 9. Comparison of the PMF factors with the fraction of the OA that is related to fossil fuel combustion. Only the days with available samples are depicted. The red dashed lines denote gaps in the collected sampling periods.

In the first period, part of the dominant LO-OOA factor was also modern (unrelated to fossil fuel combustion). In the second part of the campaign the LO-OOA factor seems to be mostly due to anthropogenic fossil combustion sources. A sensitivity test of varying the non-fossil reference value resulted in only minor changes to the estimated fraction of modern carbon (Table S3).

3.4. Particle number concentration and NPF frequency

The particle number N_4 had an average concentration of 3528 ± 1615 cm^{-3} (Figure 10), similar to particle number concentrations found in previous Greek campaigns in background sites. For example, Pikridas et al. (2010) observed around 2700 cm^{-3} in Finokalia in the summer of 2008 and Vratolis et al. (2019) around 3500 cm^{-3} during 2012. The maximum N_4 concentration was around 13000 cm^{-3} (July 13) and the minimum 750 cm^{-3} (during the rain event), while there was a notable decrease with the campaign's progression. This reduction was accompanied by an increase in the accumulation mode diameter of the mass distribution along the campaign, indicating aged transported PM. The N_4 diurnal average profile suggests a subtle increase of 570 cm^{-3} in late afternoon (Figure 6e) that follows the afternoon increase of PM_1

mass. Days exhibiting sharp increases in number included July 7 (from 4,540 cm^{-3} to 8,590 cm^{-3}), July 11 (from about 2,000 cm^{-3} to more than 7,000 cm^{-3}) and July 13 (~ 4,000 cm^{-3} up to more than 12,000 cm^{-3}). These days had an increase in the number of particles in the smaller sizes (up to 25 nm), but most of the increase was in the Aitken range of 25-100 nm (Figure S17c). Since the major increases in number do not coincide with peaks in species like BC (Figure 5) or other primary anthropogenic pollutants (NO_x and anthropogenic VOCs) they are not related to local combustion sources. These particles are probably secondary in origin, potentially related to SO_2 oxidation and sulfate formation. Sulfate levels had a modest correlation (R^2=0.34) with N_4 which increased during the high N_4 days (Figure 10), with an R^2 of 0.62 for the period up to July 14 (excluding the rain period). In the period after July 15 this correlation drops to R^2=0.14. The OA showed a milder increase during July 7 and 11 when N_4 increased, but on July 13 no increase was noted (Figure S18). This suggests a weaker link between the organics and these secondary particles. The number of larger particles (N_{100}) exhibited minimal variation during the day (Figure S17f) indicative of long-range transport. The particles smaller than 25 nm peaked at 10:00 LT on average during the campaign.

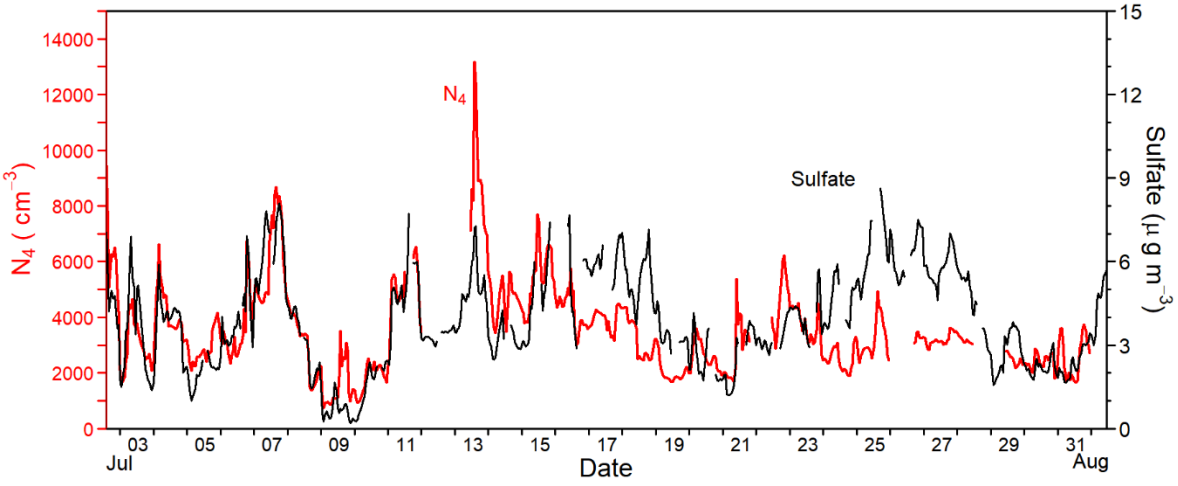

Figure 10. Hourly values of N_4 number concentration (red line) and the sulfate mass hourly variation (black line) across the campaign.

The concentrations of $N_{4\text{-}7}$ particles remained negligible during the study, suggesting no local nucleation. However, growing particle modes starting from 8-10 nm were noted for 7 days (July 7, 11, 13, 14, 20, 21, 22). These indicate new particle formation in another location relatively close to the site and subsequent transport there (Dada et al., 2018). Typical growth rates of particles in the region are 4-5 nm h^{-1} (Aktypis et al., 2024), therefore the growth to 10 nm would require nearly 2 hours. For typical morning wind speeds of 3-8 km h^{-1} in the area during the study, this suggests that the particles were formed around 5-20 km away. These

particles were typically present at around 10-11:00 LT and grew to 30-50 nm during afternoon hours. These 7 days of near-by new particle formation in a month-long period yield a frequency of 22 %.

On July 15, 16 and 25 higher diameter modes of 20-30 nm appeared later in the day (around or after midday, Figure 11), with lower growing rates. This suggests that these particles were transported from more distant areas and arrived at the site already grown (Aktypis et al. 2023).

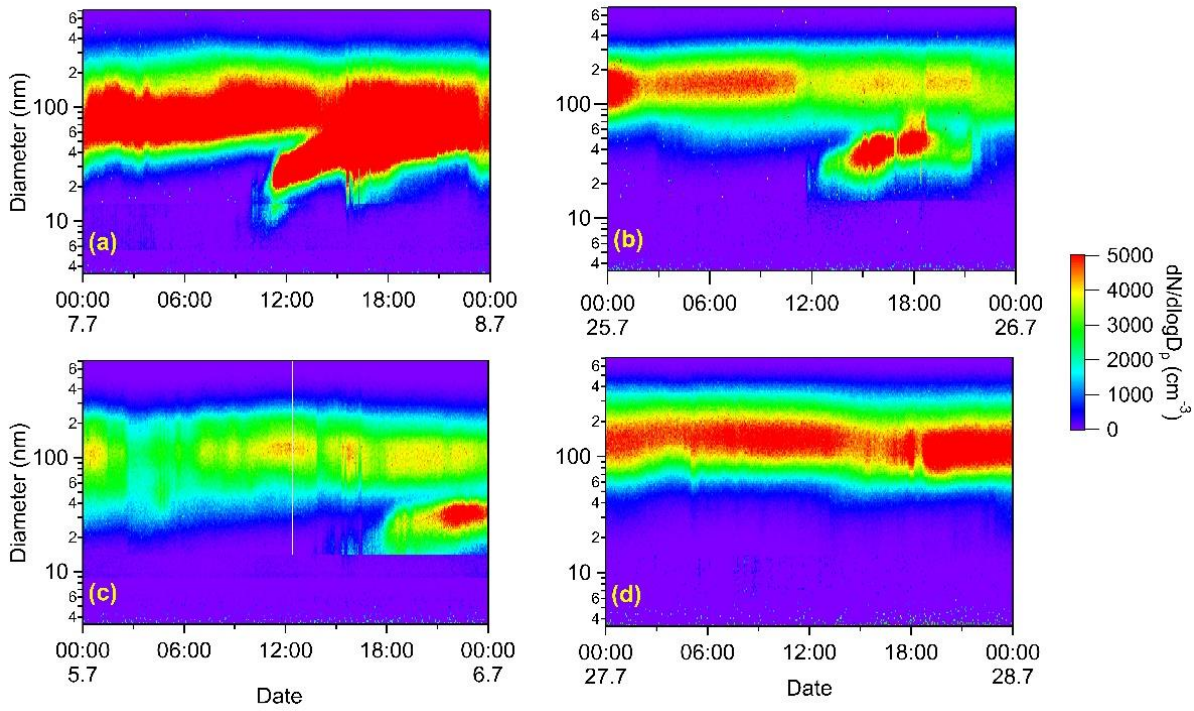

Figure 11. Typical examples of a) nearby NPF event, starting from 10 nm on July 7, b) event with appearing modes above 20 nm on July 25, c) afternoon occurrence of particles in 10-20 nm range and d) non-event in Pertouli during July 2022.

Another worth mentioning group of events had appearing particle modes at 20-50 nm after 16:00 LT lasting for the rest of the day (observed on July 3, 5, 15 and 18). These could be transported to the site from the nearby city of Trikala within a few hours (Figure S19). The remaining 17 days were non-events.

For the near-by NPF events, SO_2 reached its daily maximum at approximately the same hour as the new particles (9-11:00 LT) at levels of 0.1-1.7 ppb (Figure S20). The trajectories for the three most intense cases of near-by NPF indicated air masses passing in the vicinity of coal burning power plants in northern Greece and Northern Macedonia within a day (Figure S21).

In the event on July 20, SO_2 levels reached hourly concentrations of only 0.3 ppb, but this time the air masses came from the East (arriving locally from the NE) and the number of

particles present was smaller compared to other events (Figure S22). For the events with the 20-30 nm modes SO_2 concentrations were also elevated (1.3, 0.6 and 1.6 ppb for July 15, 16 and 25 respectively).

3.5. Concentrations of organic and inorganic gas-phase pollutants

The average ozone concentration during the campaign was at 64.8±8.3 ppb with small diurnal variation of 6 ppb or 9% (Figure 6d). The variation was more noticeable across the campaign with a minimum of 44 ppb (during the precipitation event) and a maximum of 83 ppb (Figure 12). It had a moderate correlation with PM_1 ($R^2 = 0.37$) and was better correlated with the OA ($R^2 = 0.51$).

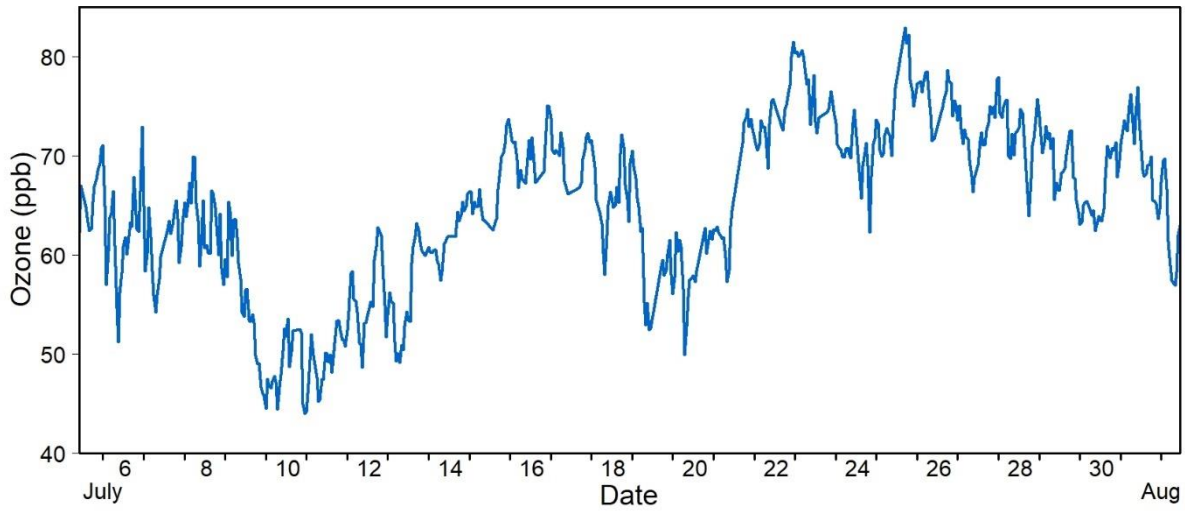

Figure 12. Hourly O_3 levels for the campaign's duration.

The average SO_2 concentration was 0.27 ± 0.30 ppb, but there were periods when it exceeded 1 ppb (Figure S20). There was no correlation ($R^2 = 0.09$) between the PM_1 sulfate and sulfur dioxide. The average SO_2/Sulfate molar ratio was low at 0.3, (Figure S23). NO_2 levels were consistently below 3 ppb, with low average levels in midday and afternoon hours (Figure 6h).

The concentrations of individual anthropogenic VOCs such as toluene (derived from *m/z* 93) and benzene (*m/z* 79) never exceeded 0.3 ppb throughout the campaign (Figure 13). However, their diurnal variation included a small peak at noon (Figure S24). This small increase (0.05 ppb for toluene, 0.03 ppb for benzene) could be due to transport from below as the boundary layer height increases. It shows that the site may have some small effects from medium distance sources. This variation was not related to air mass origin. Toluene and benzene exhibited moderate correlation with other VOCs like phenol or vinyl furan (attributed

to *m/z* 95, R^2=0.49 for benzene) and octene (*m/z* 113, R^2=0.43 for toluene, 0.46 for benzene). Other aromatics such as xylenes/ethylbenzene and benzaldehyde represented by *m/z* 107 also exhibited a peak at noun of the order of 0.1 ppb. Other aromatic compounds like benzene acetaldehyde/acetophenone/trimethyl benzenes detected on *m/z* 121 also reached 0.1 ppb during midday. Other analytes (at *m/z* of 129, 139, 155, 169 and 105) with similar diurnal profile are depicted in Figure S25.

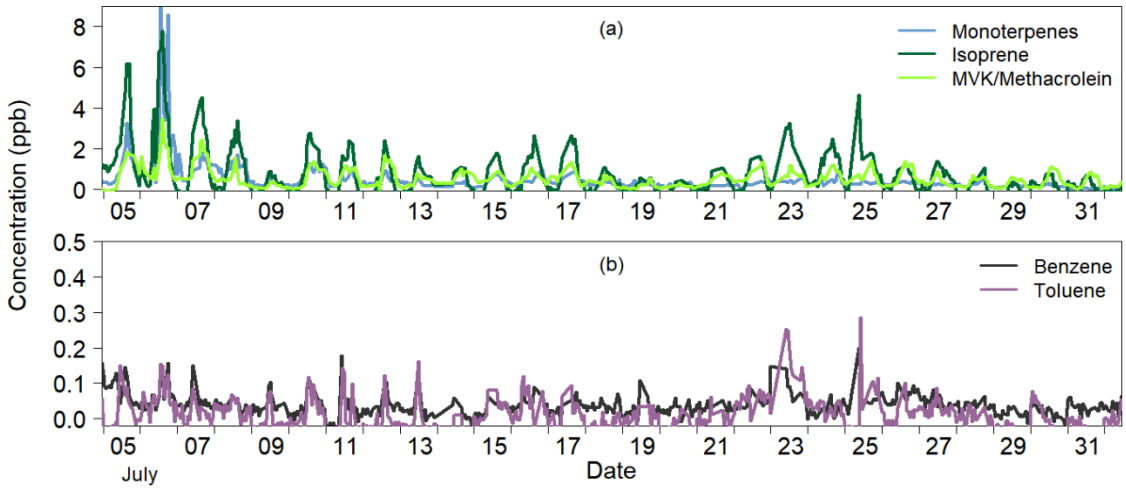

Figure 13. (a) Biogenic and (b) anthropogenic VOC hourly variation for the campaign.

Compounds of predominantly biogenic origin had higher levels during the first days of the campaign (5-7 July) (Figure 13a). The highest levels were observed in a period of lower velocity air masses at midday of July 6, when the air masses had stayed for some time in the forested areas north of the site. Isoprene (at *m/z* 69) was on average 0.65±1.12 ppb, while monoterpenes (added *m/z* 81 and 137) were 0.5±0.78 ppb. Known products of the photo oxidation of isoprene like methyl-vinyl-ketone and methacrolein (measured in *m/z* 71) had average levels equal to 0.51±0.46 ppb. Isoprene's correlation with temperature was low R^2=0.25. Methyl-ethyl-ketone, also of biogenic origin at *m/z* 73, was 0.17±0.15 ppb. After the rain event isoprene did not exceed 5 ppb. There was a general drop in the observed concentrations of the biogenics which were significantly lower after the first days of the campaign.

Identified aldehydes such as hexanal (*m/z* 101) and pentanal (*m/z* 87), methylfuran (*m/z* 83) and 1-heptene (*m/z* 99) increased by about 0.1 ppb starting at 07:00 LT and peaking at 14:00 LT (Figure S26). Their levels slowly returned to their initial values at around 20:00. They could be either directly emitted or produced by photochemical processes.

Acetone had a modest correlation with BC (R^2=0.5) and its average concentration during the campaign was 2.13 ± 0.75 ppb (Figure S27). Its diurnal average level increased by 0.55 ppb

(22%) during the day (from a minimum of 1.86 ppb at 05:00 to 2.41 at 15:00 LT), which could be a result of regional production. Acetic acid (R^2=0.52 with acetone) had an average level of 0.51 ± 0.39 ppb and had a correlation of around 0.2 with the major PM_1 constituents.

3.7. Air quality variation across sub-periods

The campaign was segregated into three periods in an attempt to infer additional information about the pollutants observed and their sources. The subperiods were selected based on the fractional contribution of the PMF factors (initial LO-OOA dominance and subsequent MO-OOA dominance), as well as based on absolute concentrations (organics and BC increased during July 14-20). The first period was from July 2 up to 13 excluding the rain period, July 14 to 20 was the second sub-period. Finally, from July 21 up to the end was the third subperiod of the campaign. The concentration distributions of the major pollutants across the three subperiods are shown in Figure 14. The biggest differences are observed for the first and third period, while the second seems to act as a transitioning period. The third subperiod had higher temperatures (by about 4 ^oC), with an increase of PM_1 by 2.7 $\mu g\ m^{-3}$ (compared to the first subperiod), mainly due to an increase in organics (and a slight increase in BC).

The LO-OOA concentration decreased by about 2 $\mu g\ m^{-3}$ (from the first to the third subperiod). Based on the average diurnal profiles during the sub periods, the LO-OOA in the first and second period had a roughly 20% contributions from regional photochemistry (Figure S28). The mostly fossil related LO-OOA of the third period had a flat diurnal profile indicative of long-range transport.

Ozone levels increased by 13 ppb (from 58 ppb in the first period to 71 ppb for the third (Figure 14i). The diurnal variation also changed between the periods (Figure S29). In the first period there is an increase of 10 ppb across the day from a minimum at 09:00 LT (when VOCs start increasing), to a maximum at 18:00 LT. The corresponding diurnal variation for the third period was halved to 5.3 ppb. There was a moderate correlation of O_3 with both the MO-OOA (R^2 = 0.53) and the bOOA factor (R^2 = 0.34), but none with the LO-OOA (R^2 = 0.01). This O_3 variation suggests that it was formed upwind by reactions that contributed also to the MO-OOA (e.g. wildfire aging). No sudden ozone changes were observed suggesting no major intrusions from the stratosphere.

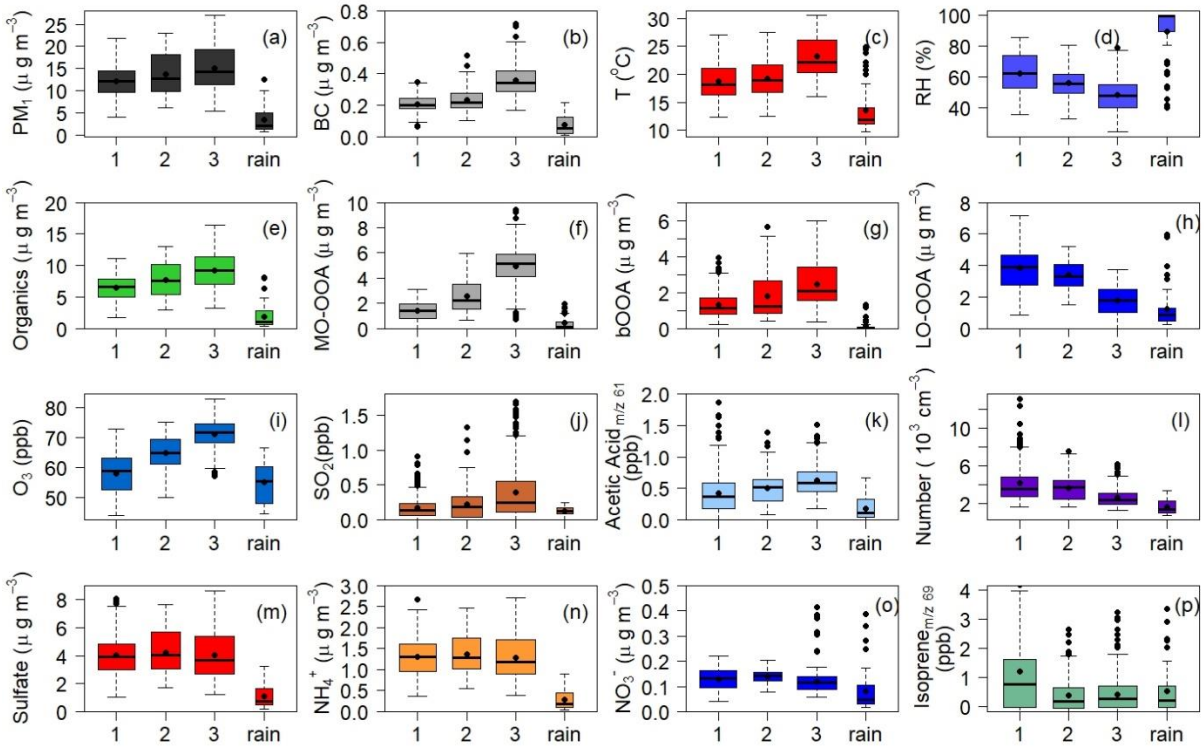

Figure 14. Boxplots of hourly pollutant distribution during different periods of the campaign. Median values are denoted by the black line (average by the dots in the box which corresponds to the interquartile range). The width of the boxes is proportional to the size of the subperiods. Period 1 is from July 2 to 13 excluding the rain period (midday of July 8 to morning of July 10). The second period covered July 14 up to July 20 and the last one went up to the end of the campaign (1st of August).

The acetone average diurnal profile in the first period showed an increase of 0.76 ppb from 06:00 LT to 14:00 LT, whereas in the third period it was flatter. Excluding the first period there was a moderate correlation of around 0.45 of acetone with both the MO-OOA and the bOOA factors, suggesting also that the observed acetone during that time was a result of transport rather than locally produced.

N_4 was lower in the third subperiod of the campaign with average hourly values of 2600 cm^{-3} after July 21, as opposed to 4200 cm^{-3} in the first subperiod and 3700 cm^{-3} in the second (Figure 14). For sulfur dioxide, higher concentrations were observed in the last subperiod.

3.8. $PM_{2.5}$ variability across Greece

The $PM_{2.5}$ values by the PANACEA low-cost sensor network (Stavroulas et al., 2020) were used to relate the $PM_{2.5}$ levels in Pertouli to those in the rest of the country (Figure S30, Table S2). Figure 15 depicts the relative homogeneity of $PM_{2.5}$ across Greece during SPRUCE-22. The local sources are apparent spikes especially in the case of urban stations but there is

clear dominance of long-range transport. It is worth noting that the center of the densely populated Athens (4 million inhabitants) had similar or even lower levels of $PM_{2.5}$ than this isolated Pertouli background site 260 km away.

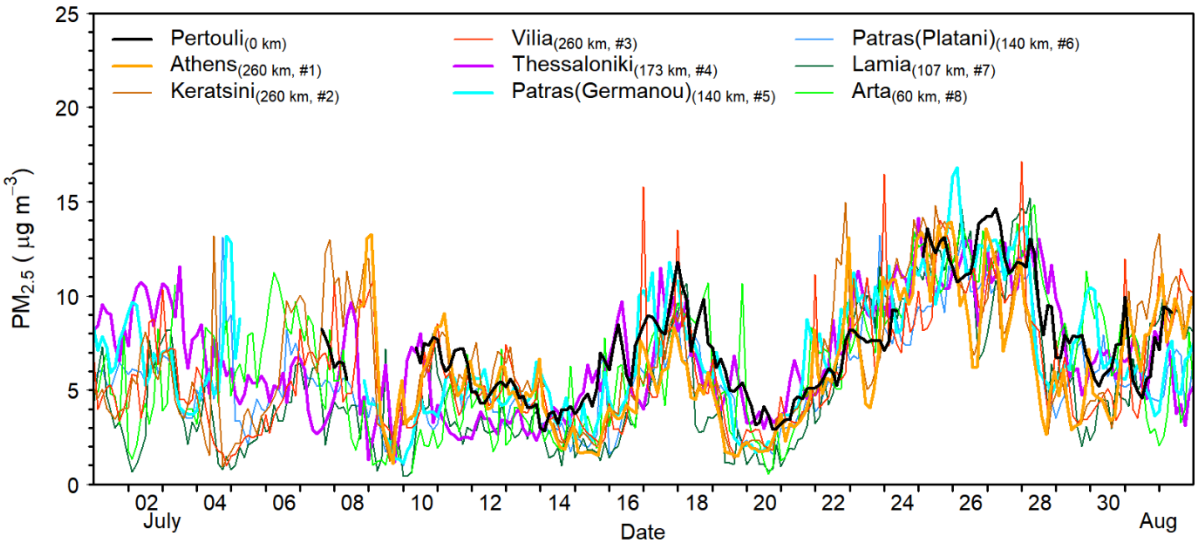

Figure 15. Background concentrations for $PM_{2.5}$ in Greece. The panel displays 3 h average concentrations of all sensors for the campaign period with the parenthesis denoting the distance to the campaign's site and the ID of the sensors in relation to the map in Figure S30.

The three stations located in and close to Athens had little variability in daily concentrations (average of 1.3 μg m^{-3}) and a maximum daily variability of 3.5 μg m^{-3} The average daily $PM_{2.5}$ concentration reported in Athens was around 1 μg m^{-3} lower than the corresponding one in Pertouli. The corresponding variability for the sensors in the city of Patras was on average 1 μg m^{-3} and their mean about 1 μg m^{-3} lower than the concentrations in Pertouli. Thessaloniki, a major city in the north of the Pertouli site had a mean difference of just 0.6 μg m^{-3} with Pertouli, while Arta the nearest station (~60 km) to the southwest reported about 0.9 μg m^{-3} less.

4. Conclusions

The campaign conducted in Pertouli aimed at the characterization of a mountainous background site under summertime conditions. PM_1 concentrations had an average of close to 13 μg m^{-3}, relatively high for a remote site. Most of the PM_1 was transported pollution rather than locally produced material, or nearby anthropogenic influences. The fact that a remote site had daily PM_1 concentrations that surpassed the 24-h $PM_{2.5}$ air quality guidelines of 15 μg m^{-3} (WHO global air quality guidelines, 2021) for 10 days out of a month indicates the significance of background aerosol in the Eastern Mediterranean during summer. $PM_{2.5}$ was homogeneously

distributed across the Greek mainland during the campaign. Local sources played a minor role in the overall fine PM levels even for large cities like Athens.

Fine particles mostly consisted of organics (~60%). The once dominant sulfate in the Eastern Mediterranean represented only 30% of the PM_1 due to stricter regulations of SO_2 emissions. The aerosol on the site was fairly processed with a high oxygen content (average O:C of 0.85) and PMF attribution showed 3 secondary oxidized factors. The highly aged particulates were well mixed with the size distribution of the PM_1 components' mass peaking at approximately the same diameter (480 nm).

The MO-OOA and bOOA levels were consistent with measured modern carbon. This supports their attribution to mostly oxidized biomass burning and aged biogenic SOA, respectively. The LO-OOA was mostly associated to fossil fuel combustion. The biogenic SOA was highly oxidized and to its majority was produced away from the site, despite its location in the middle of the forest. The chemistry has progressed past the first-generation products of the major biogenic VOCs towards highly oxidized organic molecules, during the whole campaign.

The first campaign period had higher regional photochemical activity, with higher particle number (connected to regional sulfate formation) and higher concentrations of biogenic VOCs. The dominant OA factor was the LO-OOA (with contributions from both fossil fuel related and modern carbon sources). With the campaign's progression the site was affected mostly by long range transport. The OA became mostly MO-OOA, with fewer particles but higher PM_1 concentrations. The sum of the MO-OOA and the bOOA was consistent with the non-fossil organic aerosol. Ozone levels increased and together with acetone were also related to transport during this period.

NPF did not occur directly in this site. Seven days with nearby (5-20 km away) NPF events were found. In most cases they coincided with increased SO_2 concentrations and with trajectories passing near coal burning power plants north of the site.

Authorship contribution statement

A.M.: Investigation, Methodology, Data Curation, Visualization, Writing - Original Draft. **C.N.V. K.F., A.A.:** Investigation, Data Curation, Writing - Review & Editing. **C.K.** Investigation, Methodology, Project administration, Writing - Review & Editing. **A.B. D.P., E.K., K.B. Y.F., T.T., C.P., E.B. A.N., K.SK.:** Investigation, Writing - Review & Editing. **K.SE.:** Project administration, Writing - Review & Editing. **S.N.P.:** Conceptualization, Investigation, Methodology, Supervision, Writing - Review & Editing.

Declaration of interests

The authors declare that they have no known competing financial interests or personal relationships that could have appeared to influence the work reported in this paper.

Acknowledgments

This work has received funding from the Atmospheric nanoparticles, air quality and human health (NANOSOMs) program of the Hellenic Foundation for Research and Innovation (HFRI, grant agreement no. 11504) as well as by the Chemical evolution of gas and particulate-phase organic pollutants in the atmosphere (CHEVOPIN) project (HFRI, grant agreement no. 1819). Further financial support has been provided by the Project Pyrogenic TRansformations Affecting Climate and Health (PyroTRACH, grant agreement no 726165) funded by H2020-EU.1.1-Excellent Science and the French National Research Agency (FIRETRAC project No ANR-20-CE01-0012-01). Furthermore, this publication is part of a Transnational access project that is supported by the European Commission under the Horizon 2020 – Research and Innovation Framework Programme, H2020-INFRAIA-2020-1, ATMO-ACCESS Grant Agreement number: 101008004. The authors also acknowledge the technical help provided by Maria Georgopoulou, Dontavious Sippial and Georgia Argyropoulou for completion of this work as well as the Environmental Chemical Processes Laboratory (ECPL) team in the University of Crete.

References

Aktypis, A., Kaltsonoudis, C., Patoulias, D., Kalkavouras, P., Matrali, A., Vasilakopoulou, C. N., Kostenidou, E., Florou, K., Kalivitis, N., Bougiatioti, A., Eleftheriadis, K., Vratolis, S., Gini, M. I., Kouras, A., Samara, C., Lazaridis, M., Chatoutsidou, S. E., Mihalopoulos, N., Pandis, S. N., 2024. Significant spatial gradients in new particle formation frequency in Greece during summer. *Atmos. Chem. Phys. 24*, 65–84. https://doi.org/10.5194/acp-24-65-2024

Aktypis, A., Kaltsonoudis, C., Skyllakou, K., Matrali, A., Vasilakopoulou, C. N., Florou, K., Pandis, S. N., 2023. Infrequent new particle formation in a coastal Mediterranean city during the summer. *Atmos. Environ. 302*, 119732. https://doi.org/10.1016/j.atmosenv.2023.119732

Bard, E., Tuna, T., Fagault, Y., Bonvalot, L., Wacker, L., Fahrni, S., Synal, H.-A., 2015. AixMICADAS, the accelerator mass spectrometer dedicated to recently installed in Aix-

en-Provence, France. *Nucl. Inst. Methods Phys. Res. B 361*, 80–86. https://doi.org/10.1016/j.nimb.2015.01.075

Bonvalot, L., Tuna, T., Fagault, Y., Jaffrezo, J., Jacob, V., Chevrier, F., Bard, E., 2016. Estimating contributions from biomass burning , fossil fuel combustion, and biogenic carbon to carbonaceous aerosols in the Valley of Chamonix : a dual approach based on radiocarbon and levoglucosan. *Atmos. Chem. Phys*. 16, 13753–13772. https://doi.org/10.5194/acp-16-13753-2016

Bossioli, E., Tombrou, M., Kalogiros, J., Allan, J., Bacak, A., Bezantakos, S., Biskos, G., Coe, H., Jones, B. T., Kouvarakis, G., Mihalopoulos, N., Percival, C. J., 2016. Atmospheric composition in the Eastern Mediterranean: Influence of biomass burning during summertime using the WRF-Chem model. *Atmos. Environ. 132*, 317–331. https://doi.org/10.1016/j.atmosenv.2016.03.011

Bougiatioti, A., Stavroulas, I., Kostenidou, E., Zarmpas, P., Theodosi, C., Kouvarakis, G., Canonaco, F., Prévôt, A. S. H., Nenes, A., Pandis, S. N., Mihalopoulos, N., 2014. Processing of biomass-burning aerosol in the eastern Mediterranean during summertime. *Atmos. Chem. Phys. 14*, 4793–4807. https://doi.org/10.5194/acp-14-4793-2014

Budisulistiorini, S. H., Li, X., Bairai, S. T., Renfro, J., Liu, Y., Liu, Y. J., McKinney, K. A., Martin, S. T., McNeill, V. F., Pye, H. O. T., Nenes, A., Neff, M. E., Stone, E. A., Mueller, S., Knote, C., Shaw, S. L., Zhang, Z., Gold, A., Surratt, J. D., 2015. Examining the effects of anthropogenic emissions on isoprene-derived secondary organic aerosol formation during the 2013 Southern Oxidant and Aerosol Study (SOAS) at the Look Rock, Tennessee ground site. *Atmos. Chem. Phys. 15*, 8871–8888. https://doi.org/ 10.5194/acp-15-8871-2015

Canagaratna, M. R., Jimenez, J. L., Kroll, J. H., Chen, Q., Kessler, S. H., Massoli, P., Hildebrandt Ruiz, L., Fortner, E., Williams, L. R., Wilson, K. R., Surratt, J. D., Donahue, N. M., Jayne, J. T., Worsnop, D. R., 2015. Elemental ratio measurements of organic compounds using aerosol mass spectrometry: characterization, improved calibration, and implications. *Atmos. Chem. Phys. 15*, 253–272. https://doi.org/10.5194/ acp-15-253-2015

Carslaw, D. C., Ropkins, K., 2012. Openair - An r package for air quality data analysis. *Environ. Model. Softw. 27–28*, 52–61. https://doi.org/10.1016/j.envsoft.2011.09.008

Cristofanelli, P., Landi, T. C., Calzolari, F., Duchi, R., Marinoni, A., Rinaldi, M., Bonasoni, P., 2016. Summer atmospheric composition over the Mediterranean basin: Investigation on transport processes and pollutant export to the free troposphere by observations at the WMO/GAW Mt. Cimone global station (Italy, 2165 m a.s.l.). *Atmos. Environ.* 141, 139–

152. https://doi.org/10.1016/j.atmosenv.2016.06.048

Dada, L., Chellapermal, R., Buenrostro Mazon, S., Paasonen, P., Lampilahti, J., E Manninen, H., Junninen, H., Petäjä, T., Kerminen, V. M., Kulmala, M., 2018. Refined classification and characterization of atmospheric new-particle formation events using air ions. *Atmos. Chem. Phys. 18*, 17883–17893. https://doi.org/10.5194/acp-18-17883-2018

Dayan, U., Ricaud, P., Zbinden, R., Dulac, F., 2017. Atmospheric pollution over the eastern Mediterranean during summer-A review. *Atmos. Chem. Phys*. 17, 13233–13263. https://doi.org/10.5194/acp-17-13233-2017

Diapouli, E., Popovicheva, O., Kistler, M., Vratolis, S., Persiantseva, N., Timofeev, M., Kasper-Giebl, A., Eleftheriadis, K., 2014. Physicochemical characterization of aged biomass burning aerosol after long-range transport to Greece from large scale wildfires in Russia and surrounding regions, Summer 2010. *Atmos. Environ. 96*, 393–404. https://doi.org/10.1016/j.atmosenv.2014.07.055

Draxler, R. R., Hess, G. D., 1998. An Overview of the HYSPLIT_4 Modelling System for Trajectories, Dispersion, and Deposition. *Aust. Meteorol. Mag. 47*, 295–308.

Florou, K., Liangou, A., Kaltsonoudis, C., Louvaris, E., Tasoglou, A., Patoulias, D., Kouvarakis, G., Kalivitis, N., Kourtchev, I., Kalberer, M., Tsagkaraki, M., Mihalopoulos, N., Pandis, S. N., 2024. Chemical characterization and sources of background aerosols in the eastern Mediterranean. *Atmos. Environ.* 120423. https://doi.org/10.1016/j.atmosenv.2024.120423

Georgopoulou, M. P., Camilo, J., Rodriguez, M., Hivda, C., Christos, Y., Cazaunau, M., Vasilakopoulou, C. N., Matrali, A., Seitanidi, K., Aktypis, A., Nenes, A., Buissot, C., Gratien, A., Berge, A., Pangui, E., Al Marj, E., Gerard, L., Varrault, B., Lanone, S., … Spyros, P. , 2024. A coupled atmospheric simulation chamber system for the production of realistic aerosols and preclinical model exposure. Air Qual. Atmos. Heal. 0123456789. https://doi.org/10.1007/s11869-024-01611-5

Gialesakis, N., Kalivitis, N., Kouvarakis, G., Ramonet, M., Lopez, M., Yver, C., Narbaud, C., Daskalakis, N., Mermigkas, M., Mihalopoulos, N., Kanakidou, M., 2023. A twenty year record of greenhouse gases in the Eastern Mediterranean atmosphere. *Sci. Total Environ. 864*, 161003. https://doi.org/10.1016/j.scitotenv.2022.161003

Hildebrandt, L., Engelhart, G. J., Mohr, C., Kostenidou, E., Lanz, V. A., Bougiatioti, A., Decarlo, P. F., Prevot, A. S. H., Baltensperger, U., Mihalopoulos, N., Donahue, N. M., Pandis, S. N., 2010. Aged organic aerosol in the Eastern Mediterranean: The Finokalia

Aerosol Measurement Experiment-2008. Atmos. Chem. Phys. 10, 4167–4186. https://doi.org/10.5194/acp-10-4167-201

Hua, Q., Turnbull, J. C., Santos, G. M., Rakowski, A. Z., Ancapichún, S., Pol-Holz, R. D.-H., Hammer, S., Lehman, S. J., Levin, I., Miller, J. B., Palmer, J. G., Turney, C. S. M., 2022. Atmospheric radiocarbon for the period 1950–2019. *Radiocarbon 64*, 723-745. https://doi.org/10.1017/RDC.2021.95

IONICON., 2020. *Fundamentals of PTR-MS:PTR-QMS & PTR-TOF (incl. SRI).* IONICON Analytik Ges.m.b.H. Eduard-Bodem-Gasse 3 6020, Innsbruck Austria.

Jimenez, J. L., Canagaratna, M. R., Donahue, N. M., Prevot, A. S. H., Zhang, Q., Kroll, J. H., DeCarlo, P. F., Allan, J. D., Coe, H., Ng, N. L., Aiken, A. C., Docherty, K. S., Ulbrich, I. M., Grieshop, A. P., Robinson, A. L., Duplissy, J., Smith, J. D., Wilson, K. R., Lanz, V. A., Hueglin, C., Sun, Y. L., Tian, J., Laaksonen, A., Raatikainen, T., Rautiainen, J., Vaattovaara, P., Ehn, M., Kulmala, M., Tomlinson, J. M., Collins, D. R., Cubison, M. J., Dunlea, E. J., Huffman, J. A., Onasch, T. B., Alfarra, M. R., Williams, P. I., Bower, K., Kondo, Y., Schneider, J., Drewnick, F., Borrmann, S., Weimer, S., Demerjian, K., Salcedo, D., Cottrell, L., Griffin, R., Takami, A., Miyoshi, T., Hatakeyama, S., Shimono, A., Sun, J. Y., Zhang, Y. M., Dzepina, K., Kimmel, J. R., Sueper, D., Jayne, J. T., Herndon, S. C., Trimborn, A. M., Williams, L. R., Wood, E. C., Middlebrook, A. M., Kolb, C. E., Baltensperger, U., Worsnop, D. R., 2009. Evolution of organic aerosols in the atmosphere. Science 326, 1525–1529. https://doi.org/10.1126/science.1180353

Kiendler-Scharr, A., Mensah, A. A., Friese, E., Topping, D., Nemitz, E., Prevot, A. S. H., Äijälä, M., Allan, J., Canonaco, F., Canagaratna, M., Carbone, S., Crippa, M., Dall Osto, M., Day, D. A., De Carlo, P., Di Marco, C. F., Elbern, H., Eriksson, A., Freney, E., Hao, L., Herrmann, H., Hildebrandt, L., Hillamo, R., Jimenez, J. L., Laaksonen, A., McFiggans, G., Mohr, C., O'Dowd, C., Otjes, R., Ovadnevaite, J., Pandis, S. N., Poulain, L., Schlag, P., Sellegri, K., Swietlicki, E., Tiitta, P., Vermeulen, A., Wahner, A., Worsnop, D. Wu, H. C., 2016. Ubiquity of organic nitrates from nighttime chemistry in the European submicron aerosol. *Geophys. Res. Lett. 43*, 7735–7744. https://doi.org/ 10.1002/2016GL069239

Kosmopoulos, G., Salamalikis, V., Matrali, A., Pandis, S. N., Kazantzidis, A., 2022. Insights about the sources of $PM_{2.5}$ in an urban area from measurements of a low-cost sensor network. *Atmosphere. 13,* 440. https://doi.org/10.3390/atmos13030440

Kostenidou, E., Pathak, R. K., Pandis, S. N., 2007. An algorithm for the calculation of secondary organic aerosol density combining AMS and SMPS data. *Aerosol Sci. Technol.*

41, 1002–1010. https://doi.org/10.1080/02786820701666270

Levin, I., Hammer, S., Kromer, B., Preunkert, S., Weller, R., Worthy, D. E., 2022. Radiocarbon in global tropospheric carbon dioxide. *Radiocarbon 64*, 781–791. https://doi.org/10.1017/RDC.2021.102

Lewis, C. W., Klouda, G. A., Ellenson, W. D., 2004. Radiocarbon measurement of the biogenic contribution to summertime $PM_{2.5}$ ambient aerosol in Nashville, TN. *Atmos. Environ. 38*, 6053–6061. https://doi.org/10.1016/j.atmosenv.2004.06.011

Mallet, M. D., D'Anna, B., Même, A., Chiara Bove, M., Cassola, F., Pace, G., Desboeufs, K., Di Biagio, C., Doussin, J. F., Maille, M., Massabò, D., Sciare, J., Zapf, P., Giorgio Di Sarra, A., Formenti, P., 2019. Summertime surface PM_1 aerosol composition and size by source region at the Lampedusa island in the central Mediterranean Sea. *Atmos. Chem. Phys. 19*, 11123–11142. https://doi.org/10.5194/acp-19-11123-2019

Michoud, V., Sciare, J., Sauvage, S., Dusanter, S., Léonardis, T., Gros, V., Kalogridis, C., Zannoni, N., Féron, A., Petit, J. E., Crenn, V., Baisnée, D., Sarda-Estève, R., Bonnaire, N., Marchand, N., Dewitt, H. L., Pey, J., Colomb, A., Gheusi, F., Szidat, S., Stavroulas, I., Borbon, A. Locoge, N., 2017. Organic carbon at a remote site of the western Mediterranean Basin: Sources and chemistry during the ChArMEx SOP2 field experiment. *Atmos. Chem. Phys. 17*, 8837–8865. https://doi.org/10.5194/acp-17-8837-2017

Minguillón, M. C., Ripoll, A., Pérez, N., Prévôt, A. S. H., Canonaco, F., Querol, X., Alastuey, A., 2015. Chemical characterization of submicron regional background aerosols in the western Mediterranean using an Aerosol Chemical Speciation Monitor. *Atmos. Chem. Phys. 15*, 6379–6391. https://doi.org/10.5194/acp-15-6379-2015

Mohn, J., Szidat, S., Fellner, J., Rechberger, H., Quartier, R., Buchmann, B., Emmenegger, L., 2008. Determination of biogenic and fossil CO_2 emitted by waste incineration based on $^{14}CO_2$ and mass balances. *Bioresour. Technol. 99*, 6471–6479. https://doi.org/ 10.1016/j.biortech.2007.11.042

Paatero, P., Tapper, U., 1994. Positive matrix factorization: A non-negative factor model with optimal utilization of error estimates of data values. *Environmetrics* 5, 111–126. https://doi.org/ 10.1002/env.3170050203

Panteliadis, P., Hafkenscheid, T., Cary, B., Diapouli, E., Fischer, A., Favez, O., Quincey, P., Viana, M., Hitzenberger, R., Vecchi, R., Saraga, D., Sciare, J., Jaffrezo, J. L., John, A., Schwarz, J., Giannoni, M., Novak, J., Karanasiou, A., Fermo, P., Maenhaut, W., 2015. ECOC comparison exercise with identical thermal protocols after temperature offset

correction - Instrument diagnostics by in-depth evaluation of operational parameters. *Atmos. Meas. Tech. 8*, 779–792. https://doi.org/10.5194/amt-8-779-2015

Pikridas, M., Bezantakos, S., Moˇ, G., Keleshis, C., Brechtel, F., Stavroulas, I., Demetriades, G., Antoniou, P., Vouterakos, P., Argyrides, M., Liakakou, E., Drinovec, L., Marinou, E., Amiridis, V., Vrekoussis, M., Mihalopoulos, N., Sciare, J., 2019. On-flight intercomparison of three miniature aerosol absorption sensors using unmanned aerial systems (UASs). *Atmos. Meas. Tech. 12*, 6425–6447. https://doi.org/https://doi.org/10.5194/amt-12-6425-2019

Pikridas, M., Bougiatioti, A., Hildebrandt, L., Engelhart, G. J., Kostenidou, E., Mohr, C., Prévôt, A. S. H., Kouvarakis, G., Zarmpas, P., Burkhart, J. F., Lee, B. H., Psichoudaki, M., Mihalopoulos, N., Pilinis, C., Stohl, A., Baltensperger, U., Kulmala, M., Pandis, S. N., 2010. The Finokalia Aerosol Measurement Experiment-2008 (FAME-08): An overview. *Atmos. Chem. Phys. 10*, 6793–6806. https://doi.org/10.5194/acp-10-6793-2010

Pope, C.A., Dockery, D. W., 2006 Health effects of fine particulate air pollution: Lines that connect. J. *Air Waste Manag. Assoc.* 56, 709–742. https://doi.org/10.1080/10473289.2006.10464485

Reimer, P. J., Baillie, M. G. L., Bard, E., Bayliss, A., Beck, J. W., Bertrand, C. J., Blackwell, P. G., Buck, C. E., Burr, G. S., Cutler, K. B., 2004. IntCal04 terrestrial radiocarbon age calibration, 0-26 cal kyr BP. *Radiocarbon* 46, 0–26.

Ripoll, A., Minguillón, M. C., Pey, J., Pérez, N., Querol, X., Alastuey, A., 2015. Joint analysis of continental and regional background environments in the western Mediterranean: PM_1 and PM_{10} concentrations and composition. *Atmos. Chem. Phys. 15*, 1129–1145. https://doi.org/10.5194/acp-15-1129-2015

Sciare, J., Bardouki, H., Moulin, C., Mihalopoulos, N., 2003. Aerosol sources and their Contribution to the chemical composition of aerosols in the Eastern Mediterranean Sea during summertime. *Atmos. Chem. Phys. 3*, 291–302. https://doi.org/10.5194/acp-3-291-2003

Sciare, J., Oikonomou, K., Cachier, H., Mihalopoulos, N., Andreae, M. O., Maenhaut, W., Sarda-Estève, R., 2005. Aerosol mass closure and reconstruction of the light scattering coefficient over the Eastern Mediterranean sea during the MINOS campaign. *Atmos. Chem. Phys. 5*, 2253–2265. https://doi.org/10.5194/acp-5-2253-2005

Stavroulas, I., Grivas, G., Michalopoulos, P., Liakakou, E., Bougiatioti, A., Kalkavouras, P., Fameli, K. M., Hatzianastassiou, N., Mihalopoulos, N., Gerasopoulos, E., 2020. Field

evaluation of low-cost PM sensors (Purple Air PA-II) Under variable urban air quality conditions, in Greece. *Atmosphere 11*, 926. https://doi.org/10.3390/atmos11090926

Stohl, A., Forster, C., Frank, A., Seibert, P., Wotawa, G., 2005. Technical note : The Lagrangian particle dispersion model FLEXPART version 6.2. *Atmos. Chem. Phys. 5*, 2461–2474.

Tuna, T., Fagault, Y., Bonvalot, L., Capano, M., Bard, E., 2018. Development of small CO_2 gas measurements with AixMICADAS. *Nucl. Inst. Methods Phys. Res. B 437*, 93–97. https://doi.org/10.1016/j.nimb.2018.09.012

Urdiales-Flores, D., Zittis, G., Hadjinicolaou, P., Osipov, S., Klingmüller, K., Mihalopoulos, N., Economou, T., Lelieveld, J., 2023. Drivers of accelerated warming in Mediterranean climate-type regions. *Npj Clim. Atmos. Sci. 6*, 97. https://doi.org/10.1038/s41612-023-00423-1

Vasilakopoulou, C. N., Matrali, A., Skyllakou, K., Georgopoulou, M., Aktypis, A., Florou, K., Kaltsonoudis, C., Siouti, E., Kostenidou, E., Agata, B., Nenes, A., Papagiannis, S., Eleftheriadis, K., Patoulias, D., Kioutsioukis, I., Pandis, S. N., 2023. Rapid transformation of wildfire emissions to harmful background aerosol. *Npj Clim. Atmos. Sci.* https://doi.org/10.1038/s41612-023-00544-7

Voutsa, D., Samara, C., Manoli, E., Lazarou, D., Tzoumaka, P., 2014. Ionic composition of $PM_{2.5}$ at urban sites of northern Greece: Secondary inorganic aerosol formation. *Environ. Sci. Pollut. Res. 21*, 4995–5006. https://doi.org/10.1007/s11356-013-2445-8

Vratolis, S., Gini, M. I., Bezantakos, S., Stavroulas, I., Kalivitis, N., Kostenidou, E., Louvaris, E., Siakavarasi, D., Biskosc, G., Mihalopoulos, N., Pandis, S.N., Pilinisi, C., Papayannis, A., Eleftheriadis, K., 2019. Particle number size distribution statistics at City-Centre Urban Background, urban background , and remote stations in Greece during summer. *Atmos. Environ. 213*, 711–726. https://doi.org/10.1016/j.atmosenv. 2019.05.064

Wacker, L., Christl, M., Synal, H., 2010. Bats : A new tool for AMS data reduction. *Nucl. Inst. Methods Phys. Res. B 268*, 976–979. https://doi.org/10.1016/j.nimb.2009.10.078

WHO global air quality guidelines, 2021. Particulate matter ($PM_{2.5}$ and PM_{10}), ozone, nitrogen dioxide, sulfur dioxide and carbon monoxide. Geneva: World Health Organization. Licence: CC BY-NC-SA 3.0 IGO.

Zhang, Z., Cheng, Y., Liang, L. , 2023. The measurement of atmospheric black carbon : A review. *Toxics* 11, 975. https://doi.org/https://doi.org/10.3390/toxics11120975